EES Catalysis

MINIREVIEW

View Article Online
View Journal | View Issue

Cite this: *EES Catal.*, 2024, 2, 231

Selective catalytic reduction of NO_x with NH_3 over copper-based catalysts: recent advances and future prospects

Guoquan Liu,[a] He Zhang,[a] Yi Li,[b] Pengfei Wang*[a] and Sihui Zhan*[a]

Received 20th August 2023,
Accepted 26th October 2023

DOI: 10.1039/d3ey00210a

rsc.li/eescatalysis

Selective catalytic reduction of NO with NH_3 (NH_3-SCR) is a promising technology to reduce the emission of nitrogen oxides (NO_x) from diesel engines and industrial flue gases. Due to their advantages of variable valence and high stability, Cu-based catalysts exhibit superior activity and have been widely employed in the NH_3-SCR reaction. Herein, we expound the reaction mechanism of NH_3-SCR, and summarize the comprehensive advances of Cu-based catalysts (Cu-based small-pore zeolites and Cu-containing metal oxides) developed in the last decade. In this review, the challenges and prospects for Cu-based catalysts are presented to meet the industrial need, and efficient design strategies for promoting the NH_3-SCR performance of Cu-based catalysts through support derivation, precursor optimization engineering, secondary metal doping, crystal structure regulation, preparation method modification and interaction and interface engineering are comprehensively proposed and discussed. These proposed strategies are confirmed to be beneficial for enhancing catalysis by accelerating acid and redox cycles. Besides, we sum up the poisoning mechanism of impurities from flue gas on active sites, and provide the corresponding anti-inactivation measures to inhibit the deactivation of catalysts. Finally, we hope to focus on the current opportunities and challenges faced by Cu-based catalysts, further promoting their development and achieving practical applications.

Broader context

Faced with the growing consumption of fossil fuels and consequent environmental crisis, nitrogen oxides (NO_x) remarkably influence the atmospheric environment and have become the main cause of the greenhouse effect, acid rain, photochemical smog, and $PM_{2.5}$. The selective catalytic reduction process using NH_3 (NH_3-SCR) is a promising technology to reduce the emission of NO_x from stationary and mobile sources, and Cu-based catalysts have been widely investigated as an important representative for NO_x removal. Based on the features of the NH_3-SCR reaction, this review reveals the reaction mechanisms and expounds on the design strategies of Cu-based catalysts with high catalytic activity in a targeted way, such as support derivation, precursor optimization engineering, secondary metal doping, crystal structure regulation, preparation method modification and interaction and interface engineering. Specifically, the challenges and opportunities of Cu-based SCR catalysts are presented in view of the increasing demand for SO_2/alkali metal resistance and high hydrothermal stability of catalysts. In this regard, the relevant poisoning mechanisms and anti-inactivation measures are summarized to meet industrial needs, which will indicate the future research directions and stimulate the development of novel Cu-based catalysts.

1. Introduction

1.1 NO_x pollution

Nitrogen oxides (NO_x = NO + NO_2) emitted from activities such as coal burning, motor vehicles and industrial operations are major contributors to environmental pollution,[1–3] and are associated with various forms of air pollution, including greenhouse effects, acid rain, photochemical smog, and particulate matters (PMs).[4–7] Of greater concern, NO_x will also harm the alveolar structures and capillaries of the lungs, leading to respiratory diseases in humans.[8–10] To address this issue and minimize the impact of exhaust emissions on societal development, the United States has taken initiatives to exploit technologies for reducing nitrogen oxide emissions and refine relevant laws and regulations (Clean Air Act, Sec. 407, USA, 2004). At the same time, with the rapid development of society in China, the problem of environmental pollution cannot be overlooked.

[a] *MOE Key Laboratory of Pollution Processes and Environmental Criteria Tianjin Key Laboratory of Environmental Remediation and Pollution Control, College of Environmental Science and Engineering, Nankai University, Tianjin 300350, P. R. China. E-mail: pfwang1390@gmail.com, sihuizhan@nankai.edu.cn*

[b] *Tianjin Key Laboratory of Molecular Optoelectronic Sciences, Department of Chemistry, School of Science, Tianjin University, Tianjin 300072, P. R. China*

Therefore, China has established stricter emission laws and standards for nitrogen oxides (GB13223-2011, China, 2011), regulating the emissions of power plants, natural gas-fired boilers and turbines to reach the limited emission standards. The implementation of robust policies has provided a solid foundation for reducing NO_x emissions from stationary and mobile sources.[11]

1.2 Reaction mechanism of NH_3-SCR

Recently, there have been several methods including fuel pretreatment technology, fuel combustion technology and combustion post-treatment technology to reduce NO_x emissions. Among the various aftertreatment systems, selective catalytic reduction (SCR) has emerged as the most advanced technology under investigation.[12,13] This technology utilizes suitable reducing agents such as ammonia, hydrogen[14] and hydrocarbon[15–17] to catalyze the conversion of nitrogen oxides to harmless nitrogen molecules and water. Notably, selective catalytic reduction with ammonia (NH_3-SCR) is widely employed to remove NO_x due to the advantages of wide operating temperature, superior redox properties and high thermodynamic stability.[18–22] In particular, in the real application of diesel vehicle systems (Fig. 1a), the NH_3-SCR unit is located at the downstream position of the system comprising multiple processing units. The exhaust gas traverses a complex aftertreatment system, where carbon monoxide (CO) and hydrocarbons (HCs) are oxidized and eliminated in the diesel oxidation catalyst (DOC) unit, while PMs are trapped and filtered by the diesel particulate filter (DPF).[23] Subsequently, NO molecules are converted to N_2 with reducing agents, and an ammonia oxidation catalyst (AOC) unit is used to remove the unreacted NH_3 and prevent air pollution. More and

Yi Li

Yi Li received her PhD degree in physical chemistry from Shandong University and then joined Tianjin University in 2007. Her research is directed at environmental analytical chemistry and nanomaterials and catalysis.

Guoquan Liu

Guoquan Liu is currently a PhD candidate in Prof. Sihui Zhan's group, Nankai University. His research interest is focused on environmental catalysis, including single-atom catalysis and the design of functional nanomaterials for environmental purification.

He Zhang

He Zhang currently works at the College of Environmental Science and Engineering, Nankai University. She is committed to the preparation of environmental functional materials and the improvement of experimental teaching methods.

Pengfei Wang

Pengfei Wang obtained his PhD degree at Nankai University (2018). He joined the Faculty of Environmental Science and Engineering, Nankai University (2023). His research interests focus on environmental catalysis and waste plastic valorization.

Sihui Zhan

Sihui Zhan received his PhD degree in inorganic chemistry from Shandong University and then joined Nankai University in 2007. He is now a full professor in the Faculty of Environmental Science and Engineering. He has research interests in fabrication of functional nanomaterials for water–gas purification and environmental catalysis.

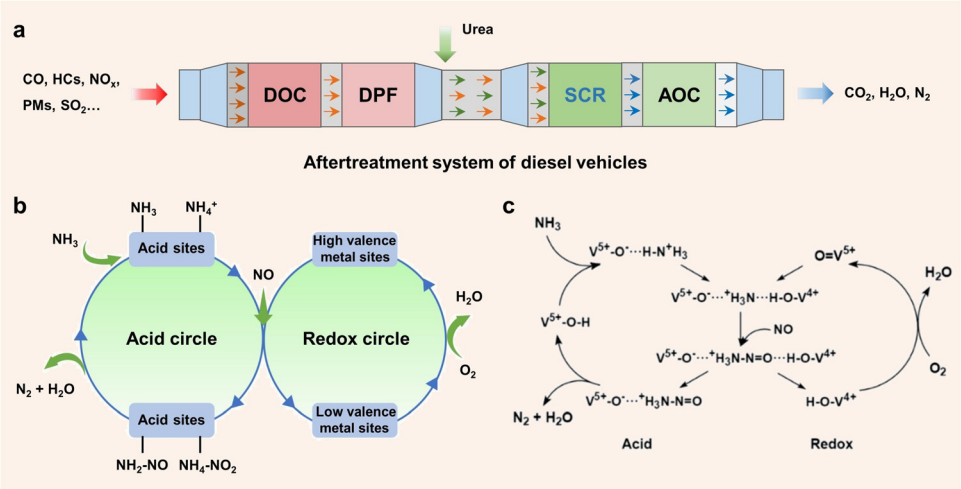

Fig. 1 (a) The after-treatment system of diesel vehicles. (b) Efficient methods for enhancing the acid cycle and redox cycle over de-NO_x catalysts. (c) The catalytic reaction diagram revealing the double cycles of the NH_3-SCR process over vanadia/titania catalysts. Copied with permission from ref. 32. Copyright 1995, Elsevier.

more studies have been focused on the NH_3-SCR process to reveal the complex reaction mechanism. In general, the reaction is generally classified into standard SCR reaction (SSCR, reaction (1)) and fast SCR reaction (FSCR, reaction (2)) based on the different ratios of NO/NO_x involved.[23–25] In the SSCR process, the N atom in NH_3 transfers $8e^-$ and $4e^-$ to NO and O_2, respectively. Oxygen molecules participate in the redox cycle and react with H atoms to form H_2O. However, the N atom in NH_3 will transfer $2e^-$ and $4e^-$ to NO and NO_2 in the FSCR reaction, in which equal amounts of NO and NO_2 are required. Besides, several main reactions may occur in the process of NH_3-SCR, as shown in eqn (3)–(5):

$$4NO + 4NH_3 + O_2 \rightarrow 4N_2 + 6H_2O \quad (1)$$

$$NO + NO_2 + 2NH_3 \rightarrow 2N_2 + 3H_2O \quad (2)$$

$$2NO_2 + 4NH_3 + O_2 \rightarrow 3N_2 + 6H_2O \quad (3)$$

$$6NO + 4NH_3 \rightarrow 5N_2 + 6H_2O \quad (4)$$

$$6NO_2 + 8NH_3 \rightarrow 7N_2 + 12H_2O \quad (5)$$

Moreover, there have been many studies concerning the catalytic path of the NH_3-SCR reaction. In general, the NH_3-SCR reaction at low temperature mainly defers to the Langmuir–Hinshelwood (L–H) mechanism. In this case, the acid sites are used for adsorbing NH_3, while NO molecules are oxidized by high-valence metal sites, leading to the formation of active nitrates or nitrites. Subsequently, NH_4NO_2 or NH_4NO_3 species are generated, which will decompose into N_2 and H_2O. During the reaction, the high-valence redox sites are firstly reduced to the low valence state and then re-oxidized by O_2, thus completing the redox cycle. Different from the L–H mechanism, researchers have suggested that the NH_3-SCR process at high temperature is more likely to follow the Eley–Rideal (E–R) mechanism. In this pathway, only NH_3 molecules are adsorbed and activated on the acidic sites of the catalysts to form NH_3 or NH_4^+ species, and then gas phase NO molecules will react with NH_3 or NH_4^+ species to form transition intermediates (NH_2NO or NH_3NO) and decompose into N_2 and H_2O.[26] It is found that the reactive intermediates formed by the L–H and E–R pathways are different, indicating that the specific reaction path can be determined by the capture of intermediates.

The double-cycle mechanisms including the redox cycle (NO_x) and acid cycle (NH_3) are of great importance in the NH_3-SCR reaction (Fig. 1b). Therefore, excellent redox properties and strong acidity are two crucial factors that determine the catalytic performance of catalysts.[27–29] In general, the redox properties of catalysts determine the low-temperature activity, while acid properties affect the activity at high temperature.[30,31] In terms of the redox cycle, efficient catalytic performance can be achieved by generating more active NO_3^-, NO_2^- and NO_2 intermediates based on the excellent redox ability. Meanwhile, strong acidity is beneficial for adsorbing and activating NH_3 molecules, facilitating the active intermediates (NH_3 or NH_4^+) to participate in the subsequent reaction with activated NO species (nitrates or nitrites species). In 1995, Topsøe *et al.* put forward a reaction mechanism involving an acid cycle and a redox cycle over V_2O_5/TiO_2 catalysts (Fig. 1c).[32,33] In the acid cycle, V^{5+}–OH sites acting as Brønsted acid sites were used for the adsorption of NH_3 molecules, and then the active H atom from NH_3 molecules was transferred to vanadium species. In this step, V^{4+}–O–H species were generated through the reduction of V^{5+}═O species, which were subsequently re-oxidized to V^{5+}═O species by O_2 in the redox cycle. The whole acid cycle was completed by the formation of N_2 and H_2O through the reaction between activated NH_3 molecules and adsorbed NO molecules. Therefore, the design of efficient SCR catalysts needs to focus on both redox and acidity properties.

1.3 Common NH_3-SCR catalysts

In view of the increasingly serious problem of environmental pollution, the use of catalytic means for effective treatment and

remediation has an important strategic significance for environmental improvement and ecological sustainable development. In this case, the application of easy and eco-friendly nanotechnology is of great significance in the process of industrialization. Nanoscale materials including oxide materials and compounds have been examined by scholars because of their unique nanostructures and extraordinary attributes.[34–37] These compounds are technologically a very beneficial kind of material because of their usage in environmental remediation.[38–40] For the NH_3-SCR reaction, catalysts such as single metal oxides, mixed metal oxides and supported metal oxides, and pure or metal-exchanged zeolites have consistently demonstrated superior de-NO_x performance and N_2 selectivity under oxygen-rich conditions, preventing the formation of secondary pollution in the NH_3-SCR.[41–45] Different catalysts have been developed to varying degrees because of their different characteristics, which are influenced by multiple effect factors (Fig. 2).[46–49] Since the late 1970s, V-based oxide catalysts have been widely explored and industrially used. However, these catalysts have several drawbacks, including a narrow working temperature window, vanadium toxicity, low SO_2-resistance performance, excessive oxidation of NH_3 and poor alkali-resistance.[50] It is well known that the SCR unit in flue gas is located before dust removers and desulfurization devices to reduce the cost of waste gas reheating. In this case, the catalyst in the flue gas is easily deactivated due to the SO_2 and flue gas poisoning. Hence, developing V-free catalysts with a broad operating window, moderate redox capacity, and high SO_2-resistance is of significance for the commercial application of NH_3-SCR technology.

Among the V-free catalysts, CeO_2-based catalysts are widely investigated owing to the superior ability to store and release oxygen, leading to the superior redox property. However, pure CeO_2 catalysts exhibit relatively weak surface acidity, which limits the activation of NH_3 and inhibits the catalytic activity.[51–53]

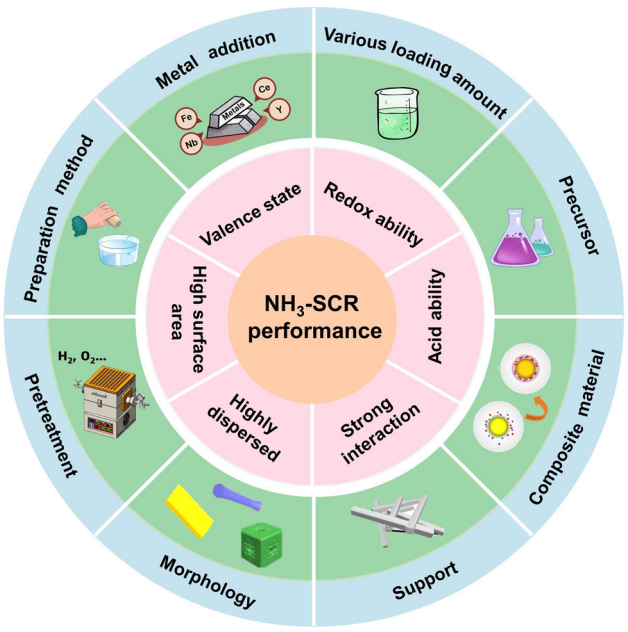

Fig. 2 Effect factors of NH_3-SCR activity.

Additionally, the superior low-temperature SCR performance of MnO_x-based catalysts has also garnered significant attention. The variable valence states of Mn species contribute to the exceptional redox ability of MnO_x-based catalysts, while pure MnO_2 catalysts have not been generalized in the industry due to their narrow operating temperature window, poor N_2 selectivity at high temperatures, and low SO_2 resistance.[54,55] Moreover, Fe_2O_3-based catalysts not only show excellent medium-high performance and SO_2-resistance at high temperatures, but also show superior thermal stability and N_2 selectivity. Nevertheless, pure Fe_2O_3 catalysts also have certain drawbacks such as a narrow operating window and relatively poor activity at low temperatures.[24,56] Consequently, substantial efforts have been made to address the limitations of current catalysts, such as introducing other transition or rare earth metal oxides to form mixed metal oxides and optimizing the structure–activity relationship, which have proven to be effective strategies.[57–59]

1.4 Cu-Based catalysts and active Cu species

Recently, Cu-based catalysts, including Cu-containing metal oxides and Cu-based small-pore zeolites, have been extensively explored in NH_3-SCR owing to the good low-temperature activity in the NH_3-SCR process.[60–62] As a transition metal, Cu species show better redox properties based on the variable valence of Cu^{2+} and Cu^{+}, which have been potential supports to combine with other foreign elements. Zhu *et al.* reported that the introduction of Nb species in CuNb binary oxide catalysts accelerated the redox reaction ($Cu^{2+} + Nb^{4+} \rightarrow Cu^{+} + Nb^{5+}$) and achieved near 100% NO conversion and N_2 selectivity (180–330 °C), resulting from increased acid amount and improved NO adsorption ability.[63] By comparison, taking CHA-type (Cu-SSZ-13 and Cu-SAPO-34), AEI-type (Cu-SAPO-18 and Cu-SSZ-39) and MFI-type (Cu-ZSM-5) zeolites as examples, Cu-based small-pore zeolites have already been applied in the commercial field due to the excellent adsorption capacity of molecule gas and enhanced catalytic performance. Generally, the small-pore CHA-type framework comprised large cavities (8.35 Å × 8.35 Å × 8.23 Å) and eight-membered ring pore windows (3.8 Å × 3.8 Å),[64] which are employed as the state-of-the-art catalysts in NH_3-SCR due to their high activity, N_2 selectivity, and excellent hydrothermal stability under harsh conditions.[65–67] Besides, AEI-type zeolites have the properties of superior low-temperature performance, wide operating windows and high N_2 selectivity. They possess a similar structure to CHA-type zeolites, characterized by an identical framework density, the presence of double six-membered ring units, and the eight-membered ring pore system with cages located at channel intersections.[68–70] For Cu-exchanged MFI-type zeolites, such as Cu-ZSM-5, they have also attracted much attention for the application of NO_x removal due to the superior stability, low cost and low toxicity.

In the catalysts mentioned above, isolated Cu species rather than CuO_x clusters are considered to be the active sites, the valence states of which have a significant effect on NH_3-SCR performance. For Cu-containing metal oxides, it is generally accepted that the interconversion between Cu^{+} and Cu^{2+} through a redox process is related to the catalytic activity.[71]

Differently, owing to the ion exchange ability of small-pore zeolites, the Cu species will be transferred to the zeolites in the form of an ionic state. Some Cu^{2+} ions interacted with two Al atoms and located at the six-membered rings of the framework (denoted as Z_2Cu^{2+}, where Z represented a zeolite framework negative charge), while the other Cu^{2+} ions formed $[ZCu^{2+}(OH)]^+$ species with a single Al atom at eight-membered rings.[72–74] Both of these Cu species attached to the zeolite framework were considered active sites in the catalytic process, with Cu^{2+} easily being reduced to monovalent Cu^+ ions, leading to the generation of new Brønsted acid sites. Thereafter, the redox cycle was completed through the oxidization process from Cu^+ species to Cu^{2+} and $[Cu(OH)]^+$ species.[75] Therefore, it was concluded that both Cu^{2+} and Cu^+ species coexisted and interconverted *via* a redox mechanism in NH_3-SCR. Although Cu-based catalysts have lots of attractive advantages presented above in the NH_3-SCR reaction, the complex operating environment still brings great challenges to the high activity, stability and anti-toxicity of catalysts.

In this work, efficient strategies for enhancing NH_3-SCR performance of Cu-based catalysts through support derivation, precursor optimization engineering, secondary metal doping, crystal structure regulation, preparation method modification and interaction and interface engineering are comprehensively summarized and discussed, and the reaction mechanisms and degradation paths of NO_x on Cu-based catalysts are pointed out. Moreover, we further conclude the toxic mechanisms of impurities on the catalysts under real applications, and put forward relevant countermeasures to improve hydrothermal resistance and poisoning-resistance (SO_2 and alkali metals) performance. In particular, for Cu-based small-pore zeolites, the hydrothermal stability needs to be further promoted because their activity always decreases significantly in the presence of water vapor at high temperatures due to the dealumination and the zeolite structure collapse. In this regard, the aim is to present an easy-to-read and comprehensive review of Cu species in NH_3-SCR, thereby highlighting the opportunities and challenges associated with Cu-based catalysts.

2. Design strategies of Cu-based catalysts and corresponding reaction mechanisms

Based on the reported research, efficient design strategies to improve the NH_3-SCR performance of Cu-based catalysts could be divided into six categories such as support derivation, precursor optimization engineering, secondary metal doping, crystal structure regulation, preparation method modification and interaction and interface engineering. Herein, we summarized the influence of each strategy on the catalytic activity and analysed the reaction mechanism and investigation status.

2.1 Support derivation

Due to the different configuration, specific surface area, electronic properties, interfacial properties, physicochemical properties, *etc.*, the supports have different effects on the chemical valence states and dispersion of Cu active species. This effect was closely related to the adsorption and activation capacity of the reactant gas molecules, which played a crucial role in the NH_3-SCR reaction (Table 1). For instance, SSZ-13, SAPO-18, SSZ-39, metal oxides, *etc.* have been widely explored as the support for efficient NO_x removal. In particular, for the commercial Cu-SSZ-13 zeolites, it had been confirmed that both monovalent- and divalent-copper sites are active centers.[76] Great efforts have been devoted to revealing the catalytic mechanism through the determination of active sites, which was helpful to provide a basis for guiding and optimizing the structure of catalysts to achieve high performance. At the same time, since the NH_3 was a gaseous reactant and H_2O was the main reaction product, a comparison was made among water-solvated and ammonia-solvated and bare Cu species to examine the impact of solvents on the activity of active Cu species (Fig. 3a). The results showed that nitrate species were more likely to be generated on solvated Cu sites during the oxidation process compared to in the absence of solvent molecules, while the reduction process of NH_3-SCR was inhibited by solvent molecules. Notably, the experimental observation of Cu-nitrate and Cu-nitrosamine (H_2NNO) spectroscopic signatures provided insights into the reaction mechanisms (Fig. 3b), and reaction mechanisms based on theoretical calculations were performed to reveal the activity of solvated active centers (Fig. 3c). Additionally, NH_3-SCR was found to follow the multisite mode on ammonia-solvated Cu species $[Cu(NH_3)_2^+]$ and Brønsted acid sites, emphasizing the importance of constructing adjacent active sites to promote the catalytic process. The solvation of NH_3 was found to assist in the generation and dispersion of Cu pairs, activating O_2 molecules and inducing the generation of HONO and H_2NNO intermediates, which were subsequently decomposed by nearby Brønsted acid sites to N_2 and H_2O (Fig. 4a).[77]

Table 1 Typical Cu-based catalysts with various supports reported in the literature

Catalysts	Reaction conditions	NO conversion	Ref.
$Cu_{1.8}$-SSZ-13	[NO] = [NH_3] = 500 ppm, [O_2] = 5%, GHSV = 400 000 h^{-1}	>40% (~240–550 °C)	78
	[NO] = [NO_2] = 250 ppm, [NH_3] = 500 ppm, [O_2] = 5%, GHSV = 400 000 h^{-1}	>90% (~240–550 °C)	
$Cu_{1.8}$-SSZ-39	[NO] = [NH_3] = 500 ppm, [O_2] = 5%, GHSV = 400 000 h^{-1}	~100% (~240–550 °C)	78
	[NO] = [NO_2] = 250 ppm, [NH_3] = 500 ppm, [O_2] = 5%, GHSV = 400 000 h^{-1}	>80% (~260–550 °C)	
Cu-SSZ-39	[NO] = [NH_3] = 500 ppm, [O_2] = 5%, [H_2O] = 5 vol%, GHSV = 19 000 h^{-1}	~90% (~250–550 °C)	79
$Cu_{2.49}$-SAPO-18	[NO] = 1000 ppm, [NH_3] = 1100 ppm, [O_2] = 5%, [H_2O] = 10 vol%, GHSV = 30 000 h^{-1}	>80% (~225–575 °C)	80
CuO/PRM	[NO] = [NH_3] = 500 ppm, [O_2] = 5%, GHSV = 120 000 h^{-1}	>80% (~275–400 °C)	86
Cu-SAPO-34	[NO] = [NH_3] = 500 ppm, [O_2] = 5%, [H_2O] = 5 vol%, GHSV = 400 000 h^{-1}	>80% (~200–550 °C)	88
Cu-ZSM-5	[NO] = [NH_3] = 500 ppm, [O_2] = 5%, GHSV = 180 000 h^{-1}	>90% (~240–350 °C)	105

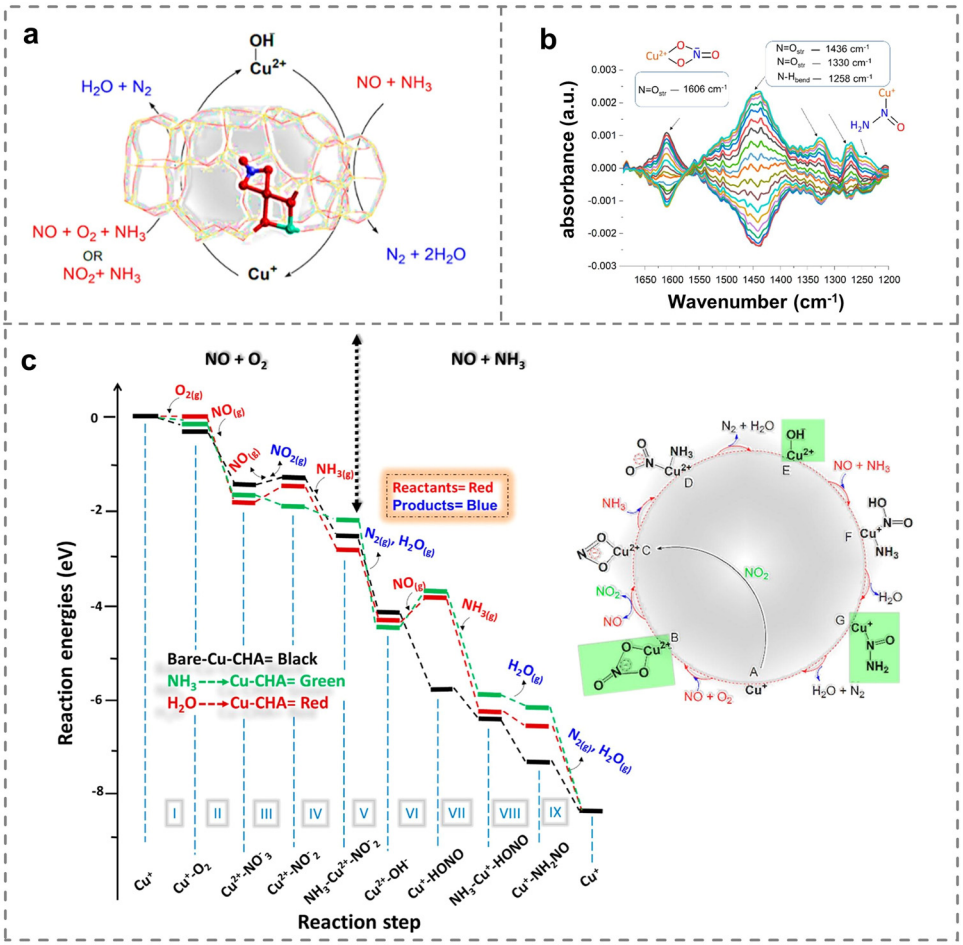

Fig. 3 (a) Schematic of the NH_3-SCR reaction mechanism on Cu-SSZ-13 zeolites. (b) Concentration modulation ME DRIFTS experiment with the corresponding phase-resolved spectrum. (c) Reaction mechanisms on the bare active site (black), ammonia-physisorbed active site (green) and water-physisorbed active site (red). Copied with permission from ref. 76. Copyright 2022, American Chemical Society.

Consequently, the researchers proposed two possible cycles to reveal the reaction path, with the difference that NO was adsorbed on ammonia-solvated Cu^+ species in cycle I while on activated oxygen in cycle II (Fig. 4b). The studies of the influence on solvated Cu-based catalysts provided a solid understand for revealing the catalytic mechanism in NH_3-SCR reactions.

Besides, Zhu *et al.* observed that Cu-SSZ-13 demonstrated excellent standard SCR performance, but they noted that the low reactivity and accumulation of NH_4NO_3 intermediates hindered NO_x conversion.[78] Particularly in the presence of NO_2, it had an inhibiting effect on the reduction of NO_x on Cu-SSZ-13, thereby limiting the process of fast SCR (Fig. 4c–e). The studies revealed that Cu-SSZ-13 catalysts exhibited fewer surface Brønsted acid sites interacting with NO_2 molecules, affecting the formation of HNO_3 species and thus decelerating the reduction of NH_4NO_3 intermediates. In contrast, a comparison with Cu-SSZ-13 catalysts demonstrated that NO_2 had the opposite effect on Cu-SSZ-39, promoting fast SCR reactions due to an abundance of surface Brønsted acid sites. The findings indicated that the choice of support played an important role in regulating the activity of the catalysts. As a result, a mass of research studies have also been devoted to improving the SCR activity of other types of Cu-based small-pore zeolites.[65,66] Fu *et al.* firstly revealed the mutual integration of framework Al atoms and Cu ions in Cu-SSZ-39 zeolites, confirming the stabilization mechanism of framework Al by Cu^{2+} ions on double six-membered ring units (Fig. 4f).[79] The content of Cu was confirmed to be closely related to the hydrothermal stability of the catalysts. Materials with higher Cu contents showed superior activity even after hydrothermal treatments at 750 and 800 °C, resulting from the framework Al being well retained by the protective effect of isolated Cu^{2+} species. However, Du *et al.* reported an unexpected promotion in the NO_x removal of aging Cu-SSZ-39 with moderate Cu contents at low temperatures. The enhancement was related to the generation of Cu_xO_y species from Cu^{2+}, facilitating the generation of nitrate species, which was different from other studies that required Cu ions for the activation of O_2 molecules and NO molecules.

Furthermore, Ming *et al.* proposed that the isolated or paired framework Al sites and Si/Al ratio were key factors determining the characteristics and the position of Cu ions in Cu-exchanged zeolites, and the catalytic performance was affected in turn. They systematically investigated the influence

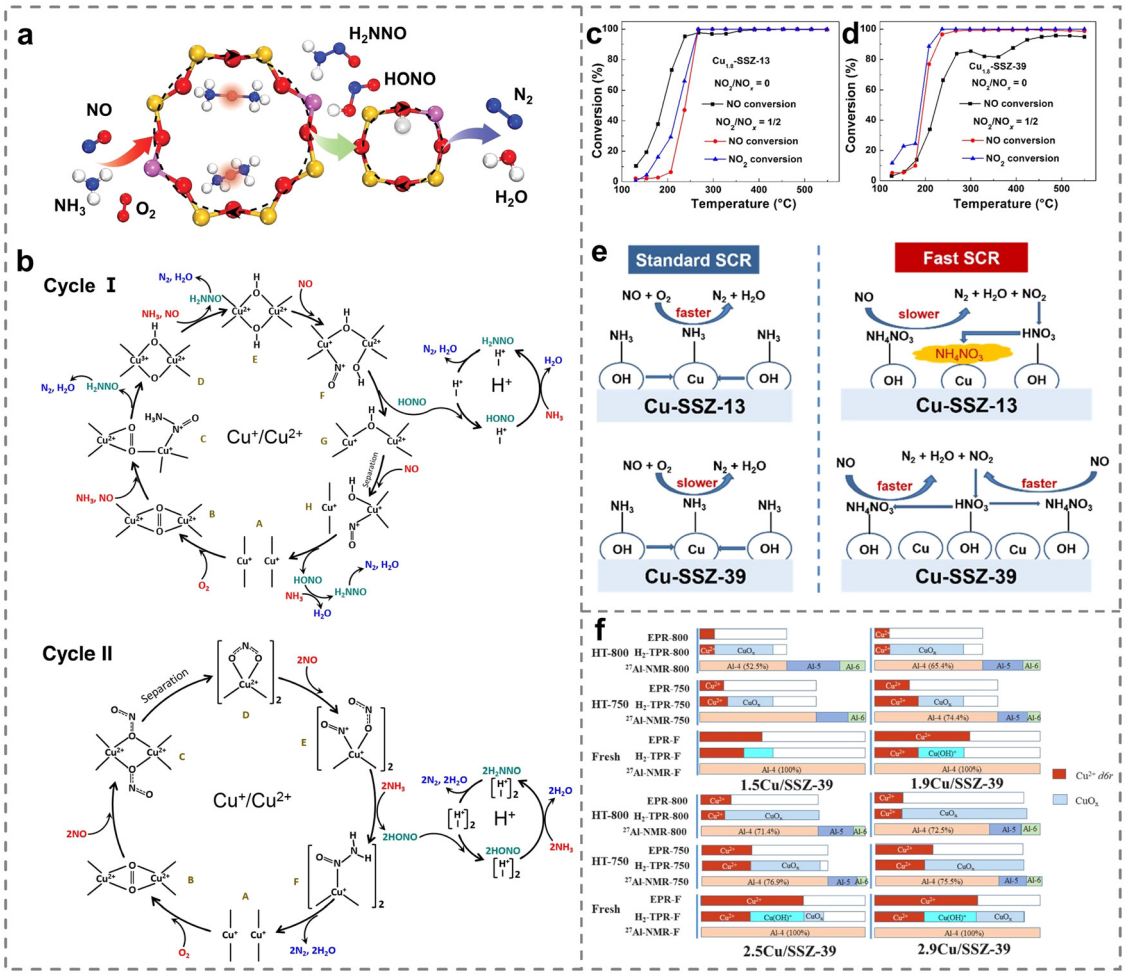

Fig. 4 (a) The reaction route in the multisite fashion for NH_3-SCR over Cu-CHA. (b) Two possible reaction mechanisms of NH_3-SCR. Copied with permission from ref. 77. Copyright 2020, American Chemical Society. (c) and (d) NH_3-SCR activity over (c) $Cu_{1.8}$-SSZ-13 and (d) $Cu_{1.8}$-SSZ-39 catalysts. (e) The influences of NO_2 on NH_3-SCR processes on Cu-SSZ-13 and Cu-SSZ-39. Copied with permission from ref. 78. Copyright 2020, American Chemical Society. (f) The contents of Al and Cu species quantified on Cu/SSZ-39 zeolites. Copied with permission from ref. 79. Copyright 2021, Elsevier.

of Cu loading and Si content on the catalytic performance of Cu-SAPO-18 catalysts.[80] By optimizing the Cu loading (1.53–3.51 wt%) and Si content (0.084–0.204), they found that the catalysts with a Cu loading of 2.49 wt% and Si content of 0.173 exhibited superior activity and hydrothermal stability. This was attributed to the generation of more acid sites and isolated Cu^{2+} ions. It was observed that when the Si content was maximum, the Cu-SAPO-18 zeolites had a large number of Si(0OAl) structures, which was not conducive to stabilizing the extra framework Cu^{2+} ions in the process of hydrothermal treatment thus leading to structural destruction. Although Cu-based small-pore zeolites had shown superior NH_3-SCR activity, complex synthesis measures and the high cost inevitably limited their further commercial application. In contrast, Cu-containing metal oxide catalysts were hopeful to be ideal candidates due to their simple preparation methods and low cost, and they have attracted significant attention for NH_3-SCR applications in recent years.[81,82] In this regard, various selections of supports were expected to enhance the catalytic performance in the NH_3-SCR process.[83–85] For instance, pretreated raw mud (PRM) was used as a support, and then CuO/PRM catalysts were synthesized by introducing varying CuO contents.[86] The results showed that 7 wt% CuO promoted the redox equilibrium of $Cu^{2+} + Fe^{2+} \leftrightarrow Cu^+ + Fe^{3+}$ and induced more Cu^+ and surface oxygen active species. The enhanced Eley–Rideal mechanism was further facilitated by the competitive adsorption between NO_x and NH_3 molecules, as the dispersed CuO improved NH_3 adsorption but weakened NO_x adsorption. Therefore, the role of the support in affecting the active sites and reaction mechanism could not be ignored, so choosing a suitable support was an effective strategy to regulate the performance of active centers, optimize the reaction path and maximize the activity.

2.2 Precursor optimization engineering

The synthesis of zeolites was closely related to different types of Si sources and Cu sources of the precursors. It had been well verified that the formation of different sizes of aluminosilicate intermediates and primary nucleus would be greatly regulated by optimizing the Si source precursor, which further affected

the nucleation and crystallization process. For instance, the structural characteristic of the SSZ-13 support would be significantly tuned by precursor optimization engineering (Fig. 5a), in which various Si sources such as colloidal silica (Si sol), gelatinous silica (Si gel) and tetraethyl orthosilicate (TEOS) were chosen as the precursors, thus leading to variations in acidity and the distribution of Cu species over Cu-SSZ-13.[87] Cu-SSZ-13 zeolites prepared with silica sol (CS-Si sol) showed more uniform sizes and high surface areas, which promoted the adsorption of reactants. Meanwhile, more Cu^{2+} active species were detected on the CS-Si sol catalysts, resulting in superior hydrothermal stability after the same hydrothermal treatment. Moreover, different Cu sources had significant effects on the type and distribution of active sites in the NH_3-SCR reaction. Then, the influence of various Cu precursors on the catalytic activity of Cu-SAPO-34 zeolites was further explored. The physicochemical properties of various Cu-SAPO-34 catalysts with different precursors of Cu (A: Cu-acetate; N: Cu-nitrate; Cl: Cu-chloride; and S: Cu-sulfate) were employed to reveal the underlying phenomena and essence of the catalytic process.[88] This study demonstrated that Cu(A)-SAPO-34 zeolites exhibited the best catalytic performance compared to Cu(N, Cl or S)-SAPO-34 zeolites. This would be attributed to the presence of a higher proportion of isolated Cu^{2+} species and fewer CuO species on the Cu(A)-SAPO-34 catalysts. Unfortunately, all aged catalysts experienced a decrease in activity after hydrothermal treatment, as a portion of isolated Cu^{2+} ions became unstable and then transformed into CuO species, resulting in catalyst deactivation. In this regard, submicron Cu-SAPO-34 catalysts, prepared by combining Cu-TEPA and morpholine as templates, exhibited superior catalytic performance and hydrothermal stability compared to the reference catalysts using Cu-TEPA, diethylamine and tetraethylammonium bromide as templates.[89] The presence of Si(nOAl) (n = 1–4) structures in Cu-SAPO-34 triggered the generation of a significant number of Brønsted acid sites and enhanced NO_x reduction. Besides, the isolated

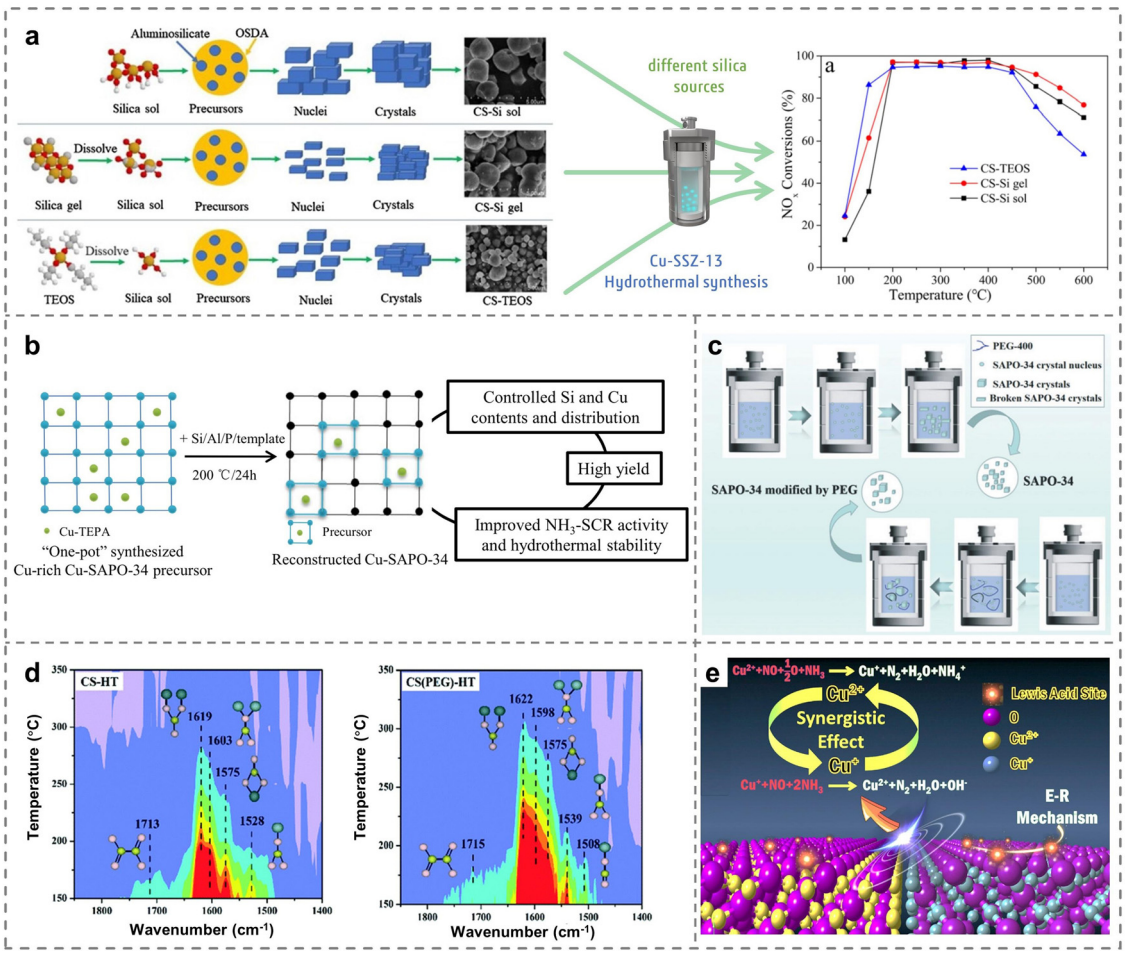

Fig. 5 (a) Schematic diagram of the proposed pathways of SSZ-13 crystallization (Si: yellow, O: red, C: gray, H: white) and NH_3-SCR performance of Cu-SSZ-13 prepared through using different Si sources. Copied with permission from ref. 87. Copyright 2020, Elsevier. (b) The reconstruction approach for the preparation of Cu-SAPO-34. Copied with permission from ref. 94. Copyright 2020, Elsevier. (c) The crystallization of SAPO-34 and the process induced by PEG. (d) NO + O_2 adsorption spectra of SAPO-34 and PEG-modified SAPO-34 zeolites after the hydrothermal treatment (pink ball presents oxygen atom, yellow ball presents nitrogen atom, and blue ball stands for copper atom). Copied with permission from ref. 95. Copyright 2021, Royal Society of Chemistry. (e) Catalytic mechanism of catalysts prepared with Cu-MOFs as the precursor. Copied with permission from ref. 96. Copyright 2019, Elsevier.

Cu^{2+} ions were effectively preserved and stabilized by Si(*n*OAl) components, which was critical in the development and manufacture of Cu-SAPO-34 SCR catalysts to achieve superior activity and hydrothermal stability for commercial applications.

Although Cu-SAPO-34 zeolites with CHA framework topology have garnered considerable attention because of the remarkable NH_3-SCR performance across a broad operating temperature range and high-temperature hydrothermal stability,[90,91] the crystallinity of Cu-SAPO-34 zeolites tended to decline during the process of traditional metal ion loading in the repeated ion exchange. The other main issue arrived when copper-tetraethylenepentamine (Cu-TPEA) was used as the structure-directing agent, as it often led to the production of high Si contents and numerous Si islands on Cu-SAPO-34 through the one-pot method, significantly reducing the catalytic activity and hydrothermal stability.[68,92,93] In response, Sun *et al.* proposed a reconstruction approach for synthesizing Cu-SAPO-34 *via* using Cu-rich SAPO-34 as the Cu precursor.[94] This approach offers advantages such as a wider crystallization phase region, high yield and adjustable contents of Si and Cu components compared to the traditional ''one-pot'' means (Fig. 5b). The resulting Cu-SAPO-34 zeolites exhibited a higher content of isolated Cu^{2+} after undergoing high-temperature hydrothermal treatment. Notably, the low-silica catalysts retained their acid sites, which contributes to superior hydrothermal stability.

Additionally, polyethylene glycol (PEG) was of great importance to the nucleation and crystal growth of zeolites, and thus intact hierarchical PEG-modified Cu/SAPO-34 catalysts were prepared to enhance the hydrothermal stability for NH_3-SCR.[95] The chain-like PEG micelles synthesized by the traditional hydrothermal method would provide sufficient space for crystal growth by adhering to and wrapping SAPO-34, forming large SAPO-34 crystals of 3–7 μm (Fig. 5c). The key intermediates of bridged nitrates (1598/1622 cm^{-1}) induced by NO activation were detected on adjacent isolated Cu sites, which was beneficial for the dissociation of O_2 and promoted the reduction of NO_x on PEG-modified catalysts after the hydrothermal aging (800 °C for 12 hours with 10 vol% H_2O) (Fig. 5d). Except for Cu-based small-pore zeolites, Wang *et al.* prepared Cu metal organic frameworks (MOFs) with a porous CuO/Cu_2O heterostructure by regulating Cu precursors.[96] On the one hand, the amount of oxygen defects increased in the CuO/Cu_2O heterostructure, enabling efficient O_2 adsorption. On the other hand, the synergistic effect between Cu^+ and Cu^{2+} led to the presence of more Lewis acid sites compared to bulk CuO and Cu_2O, facilitating the E–R mechanism of the NH_3-SCR reaction (Fig. 5e). Therefore, the preparation of catalysts with high performance through precursor optimization engineering was of great significance to the promotion of Cu-based catalysts in industrial applications.

2.3 Secondary metal doping

Due to being limited to the sole Cu active sites, the strategy of doping secondary metals was efficient to improve the catalytic activities of Cu-based catalysts (Table 2). For example, the low-temperature activity on Cu-SSZ-13 could be promoted through the introduction of Nb species.[97] After Nb species entered the exchange sites of the framework, both Lewis acid sites and Brønsted acid sites were enhanced, promoting the adsorption of NH_3 molecules. Meanwhile, more NO_x species could adsorb on Nb-modified Cu-SSZ-13 catalysts and react with NH_4^+ species adsorbing on Brønsted acid sites *via* the Langmuir–Hinshelwood mechanism. It is well-known that the rare earth metals acting as promoters had a superior regulation function on the reactivity of active centers and performance of catalysts. As expected, a crucial study discovered that a series of Cu-Sm-SSZ-13 catalysts exhibited enhanced low-temperature activity (Fig. 6a).[98] Sm ions were observed to be present at six-membered rings of SSZ-13, and then the influence of Sm ions was thoroughly investigated. The theoretical results revealed that the introduction of Sm species facilitated the formation of $[ZCu^{2+}(OH)]^+$ ions and promoted their activity, further reducing the formation energies of active NH_4NO_2 (14.9 *vs.* 18.5 kJ mol^{-1}) and H_2NNO (39.5 *vs.* 69.7 kJ mol^{-1}) components in the NH_3-SCR process (Fig. 6b and c). Notably, the strong electrostatic interaction between Sm^{3+} and $[ZCu^{2+}(OH)]^+$ also restrained the formation of inactive CuO_x species, resulting in the high stability of Cu-Sm-SSM-13 catalysts. Similarly, after the introduction of La species into the Cu-SSZ-13 zeolites, the Cu-La-SSZ-13 exhibited a higher hydrothermal stability (aging in the flowing air containing 10 vol% H_2O at 750 °C for 16 h) than that of Cu-SSZ-13, resulting from the incorporation of La ions inhibiting the transformation from Z_2Cu^{2+} to inactive CuO_x species and protecting the framework of zeolites (Fig. 6d).[99] To further reveal the promotion effect of La species, the transition process from Z_2Cu^{2+} to $Cu(OH)_2$ by the damage of water was carried out with DFT calculations. When La species existed, the formation barrier of $Cu(OH)_2$ was higher (221.5 kJ mol^{-1}) than that of 113.5 kJ mol^{-1} in the absence of La species (Fig. 6e), indicating that the generation of CuO_x inactive species was well inhibited.

Table 2 Representative Cu-based catalysts modified with secondary metal doping for the SCR reaction

Catalysts	Reaction conditions	NO conversion	Ref.
Nb/Cu-SSZ-13	[NO] = [NH_3] = 500 ppm, [O_2] = 5%, [H_2O] = 10 vol%, GHSV = 60 000 h^{-1}	>80% (~175–650 °C)	97
Cu-Sm-SSZ-13	[NO] = [NH_3] = 500 ppm, [O_2] = 5%, [H_2O] = 5 vol%, GHSV = 200 000 h^{-1}	>90% (~200–550 °C)	98
Cu-Sm-SSZ-13	[NO] = [NH_3] = 500 ppm, [O_2] = 5%, [H_2O] = 5 vol%, GHSV = 200 000 h^{-1}	>90% (~200–550 °C)	99
$Cu_yCe_{1-y}W_5O_x$	[NO] = [NH_3] = 500 ppm, [O_2] = 5%, GHSV = 36 000 h^{-1}	>80% (~240–390 °C)	102
Cu/Y-SSZ-39	[NH_3] = 220 ppm, [NO] = 200 ppm, [O_2] = 10%, [H_2O] = 5 vol%, GHSV = 40 000 h^{-1}	>70% (~200–550 °C)	103
MnCu-SSZ-39	[NO] = [NH_3] = 500 ppm, [O_2] = 5%, GHSV = 150 000 ml g^{-1} h^{-1}	>80% (~250–550 °C)	104
FeCu-ZSM-5	[NO] = [NH_3] = 500 ppm, [O_2] = 5%, GHSV = 180 000 h^{-1}	>90% (~230–500 °C)	105
Mo/CuO	[NO] = [NH_3] = 500 ppm, [O_2] = 3%, GHSV = 45 000 h^{-1}	>80% (~175–275 °C)	84

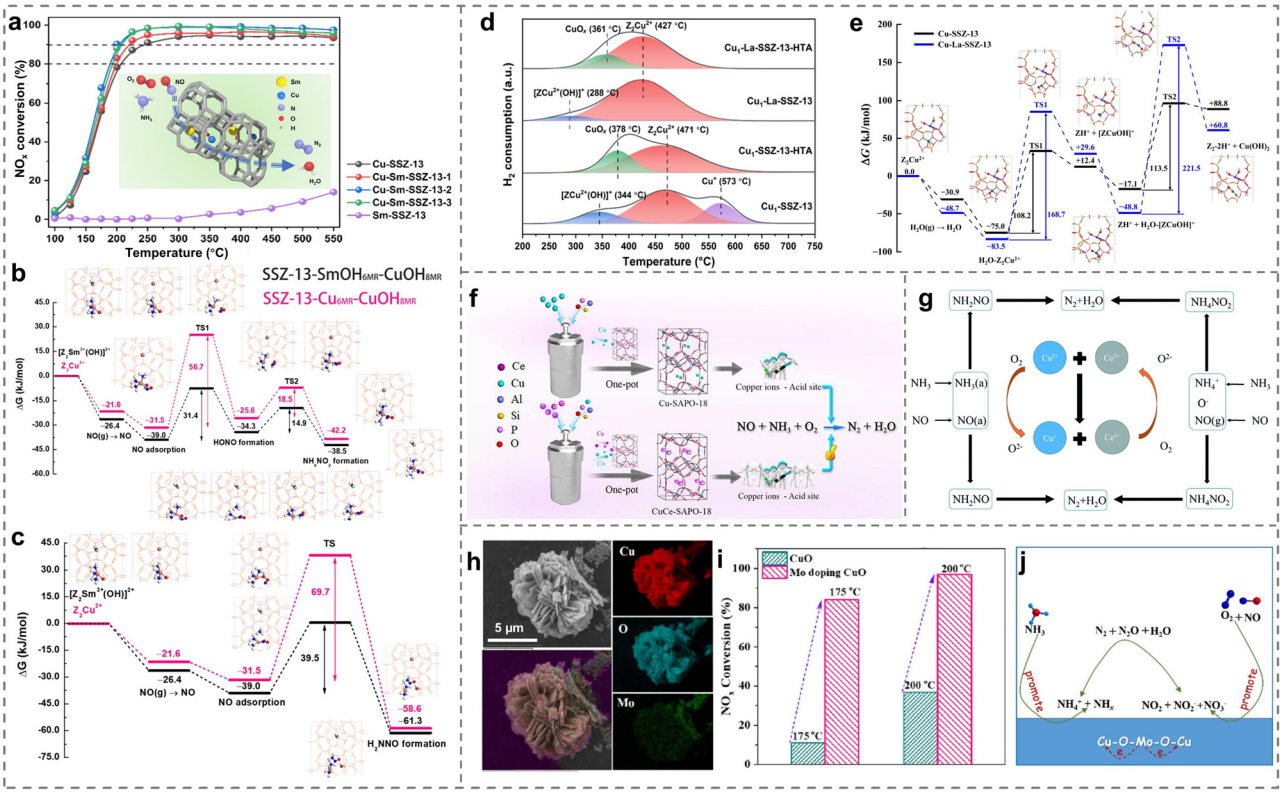

Fig. 6 (a) NH_3-SCR performance of Cu-SSZ-13 and Sm-doped Cu-SSZ-13 catalysts. (b) and (c) Generation of (b) NH_4NO_2 and (c) H_2NNO on $Cu^{2+}(OH)(NH_3)_3$ with $[Z_2Sm^{3+}(OH)]^{2+}$ and Z_2Cu^{2+}, and corresponding intermediates. Copied with permission from ref. 98. Copyright 2022, American Chemical Society. (d) H_2-TPR profiles of the as-prepared catalysts before and after hydrothermal ageing. (e) The conversion of Z_2Cu^{2+} species in the absence or presence of $[ZLa^{3+}(OH)_2]^+$ under hydrothermal treatment. Copied with permission from ref. 99. Copyright 2023, Springer Nature. (f) The schematic diagram regarding the catalyst synthesis process. Copied with permission from ref. 100. Copyright 2022, Elsevier. (g) The interaction of Cu and Ce species over $Cu_yCe_{1-y}W_5O_x$ composite materials. Copied with permission from ref. 102. Copyright 2019, Royal Society of Chemistry. (h) Mapping images of Mo-doped CuO catalysts. (i) NH_3-SCR performance of the as-prepared catalysts. (j) The mechanism of Mo-doped CuO catalysts. Copied with permission from ref. 84. Copyright 2022, Elsevier.

Notably, as the metal dopants, Ce species exerted a remarkable modifying effect on Cu-SAPO-18 zeolites. Therefore, plenty of effort has been made to explore the promotion mechanism of Ce ions. Wu *et al.* reported that the doping of Ce and Cu in SAPO-18 catalysts (CuCe-SAPO-18) influenced the distribution of Si atoms and the coordination of Al atoms in the skeleton structure,[100] which increased the quantity of active Cu^{2+} ions and the acid sites of the catalysts (Fig. 6f), leading to the significant increase of catalytic activity at low temperatures (<200 °C). In one similar study, Han *et al.* proposed that the rate of Langmuir–Hinshelwood and Eley–Rideal route accelerated by doping Ce might be the main reason for superior performance.[101] Importantly, the synergistic effects between Cu and Ce were revealed to enhance the reducibility and surface acid property of the composite materials ($Cu_yCe_{1-y}W_5O_x$), which was facilitated by the conversion of Cu^{2+}/Ce^{3+}–Cu^{+}/Ce^{4+} coupled redox ion pairs (Fig. 6g).[102]

Moreover, other transition metals such as yttrium ions (Y^{3+}) were found to be conducive to improving the hydrothermal stability of Cu/SSZ-39 at higher temperatures (>800 °C).[103] Y^{3+} ions were confirmed to enter into the cages of SSZ-39 zeolites on the modified catalyst (Cu/Y-SSZ-39), which induced more isolated Cu ions in the double six-membered rings of SSZ-39 zeolites, showing remarkably higher NO_x conversion and hydrothermal stability than Cu/SSZ-39. Wang *et al.* even confirmed that Mn species were more beneficial in improving the catalytic activity of Cu-SSZ-39 than Ce species after the hydrothermal treatment.[104] Compared to pure Cu-SSZ-39, the introduction of Mn not only inhibited cluster aggregation but also accelerated the formation of isolated Cu^{2+} species. Meanwhile, the structure and acid density were well preserved on MnCu-SSZ-39 even after hydrothermal treatment at temperatures as high as 850 °C, thus improving NH_3-SCR performance. Similarly, the addition of Fe species would broaden the temperature window and promote the hydrothermal stability of FeCu-ZSM-5 compared to reference catalysts (Cu/ZSM-5 and Fe/ZSM-5).[105] This improvement could be attributed to the hierarchical micro-mesoporous structures exhibited by the FeCu-ZSM-5 catalysts prepared *via* the one-pot method, which facilitated the dispersion of Cu active sites on the surface. In addition, various contents of Ag were employed to dope on Cu/ZSM-5 catalysts to regulate defects by utilizing the synergistic effect between Ag and Cu atoms.[106] On the one hand, $Ag_{1.5}$-Cu/ZSM-5 catalysts enhanced the adsorption of NH_3 molecules owing to the

enhanced surface acidity resulting from the introduction of Ag. On the other hand, the interaction between Ag and Cu species was revealed, leading to the generation of more active oxygen species on the catalysts and consequently contributing to improved redox performance.

Besides, for Cu-based metal oxides, the introduction of Mo to the CuO support induced the formation of the Mo–O–Cu structure, and then a large number of acidic sites and oxygen vacancies were produced through the electron interaction between Mo and Cu species.[84] This promoted the adsorption of NH_3 and NO, thereby forming active intermediates such as nitrate, nitrite, NH_3 and NH_4^+, which improved the SCR performance (Fig. 6h–j). The results well explained the important role of secondary metal doping on the enhanced performance of Cu-based catalysts.

2.4 Crystal structure regulation

Different crystal structures such as crystallite size, exposed crystal plane and morphology would affect the active site, electronic structure, acidity and redox properties of the catalysts, which was closely related to the catalytic performance. Therefore, the efficient removal of NO_x would be realized through regulation engineering of the crystal structure on the Cu-based catalysts, and it was of guiding significance for the in-depth understanding of the reaction mechanism and the development of high-performance catalysts.

Recently, it was generally believed that the smaller the size of the active centers, the higher the utilization of atoms, which would better promote the catalytic performance. In this regard, Huang *et al.* regulated Cu-SAPO-34 zeolites with different crystallite sizes (1–13 μm) and confirmed that the rate of NH_3-SCR reaction tended to decrease with the increase of the Cu-SAPO-34 crystallite size. In addition, a battery of Cu-ZSM-5 catalysts possessing micro-fibrous structures has been shown to help improve the acidic properties when the molar ratio of Si/Al was 100.[107] And the utilization of mesoporous ZSM-5 zeolite (MZ) for supporting Cu and Ce atoms (Cu–Ce/MZ) led to the detection of more highly distributed active sites and abundant oxidation species, thus yielding better performance compared to conventional Cu–Ce/ZSM-5 and Cu–Ce/SBA-15.[108] Therefore, the crystal structure regulation of ZSM-5 zeolite is important in tailoring SCR catalysts for effective removal of NO_x. Besides, the morphologies of ZSM-5 zeolites has also been confirmed to be associated with the catalytic performance of NH_3-SCR.[109] Distinct differences in SCR behaviour were observed between traditional Cu-ZSM-5 and specialized Cu-ZSM-5 zeolites with various morphologies (nanoparticles, nanosheets and hollow spheres) (Fig. 7a). Among them, nanosheet-like Cu-ZSM-5 catalysts exhibited the most superior activity, with a T_{50} as low as 130 °C and almost 100% NO_x conversions from 200 to 400 °C (Fig. 7b). It was discovered that adequate mesoporous and framework Al atoms existed on the

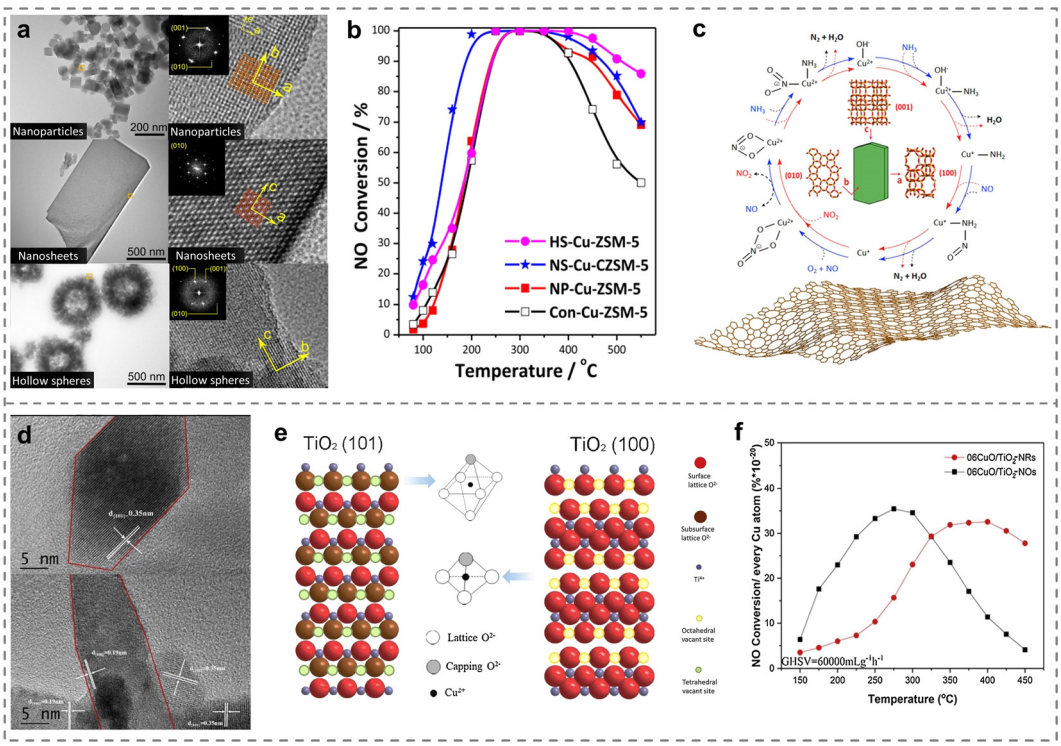

Fig. 7 (a) TEM images of Cu-exchanged catalysts with different morphologies (NP, NS and HS). (b) NO_x conversion over various as-prepared catalysts. (c) Catalytic mechanism of the NH_3-SCR process on NS-Cu-ZSM-5. Copied with permission from ref. 109. Copyright 2021, American Chemical Society. (d) HRTEM and (e) schematic diagram for TiO_2 with different exposed facets: TiO_2 (101), TiO_2 (100), and Cu cation in octahedral vacant sites and in tetrahedral vacant sites. (f) NH_3-SCR performance over different TiO_2 supports modified by CuO (06CuO/TiO_2-NOs and 06CuO/TiO_2-NRs). Copied with permission from ref. 110. Copyright 2020, Elsevier.

nanosheet-like Cu-ZSM-5, which influenced the local environment of Cu through rapid switching between Cu^{+} and Cu^{2+} ions in the catalytic process, thereby resulting in the best SCR activity. Furthermore, they revealed the reaction mechanism that the NH_3-SCR reaction over Cu-ZSM-5 nanosheets mainly followed the Eley–Rideal pathway (Fig. 7c). Different exposed crystal planes on metal oxides would affect the number and distribution of interfacial active species and defects of catalysts, and then regulated the coordination structure of the active sites. The loading of CuO phase onto the surface of the TiO_2 nano-octahedra (06CuO/TiO_2-NOs) and nano-rods (06CuO/TiO_2-NRs) using the impregnation method has been reported.[110] The different coordination environments of Cu species induced by various exposed crystal facets of TiO_2 nano-octahedra and nano-rods played a crucial role. Specifically, Cu ions were present at tetrahedral vacant sites on the (101) plane of the TiO_2 nano-octahedra and bonded to four O atoms, while on the (100) facet of TiO_2 nano-rods, they occupied octahedral vacant sites and coordinated with six oxygen atoms (Fig. 7d and e). The unique nano-octahedron structure enhanced de-NO_x activity by promoting the redox cycle of $Cu^{2+} + Ti^{3+} \leftrightarrow Cu^{+} + Ti^{4+}$ and generating more acid sites (Fig. 7f). Based on these cases, it was urgent to develop the strategy of crystal structure regulation to controllably synthesize Cu-based catalysts to understand the relationship of structure and activity deeply, expanding the applications in NH_3-SCR reaction.

2.5 Preparation method modification

Generally, the metal dispersions, valence states and de-NO_x activity were related to the preparation method. Therefore, the modification and optimization of the synthetic techniques directly tuned the structure–activity relationship of Cu-based catalysts, and thus maximized the catalytic performance (Table 3).[111] The synthesis strategies of incipient wetness impregnation (IWI), ion exchange (IE) and hydrothermal synthesis (HTS) have been extensively explored by Han *et al.* for obtaining Cu-SSZ-13 catalysts (Fig. 8a).[112] Comprehensive results demonstrated that a larger number of stable Cu^{2+} active sites was located in the six-membered rings on Cu-SSZ-13 (HTS) catalysts compared to catalysts prepared by the other two methods, leading to the highest NH_3-SCR activity (above 90% NO_x removal at 215–600 °C) because of the better abilities for NH_3 and NO adsorption. However, the traditional hydrothermal preparation methods were difficult to control the composition and structure of the samples. An alternative route called the microwave-assisted hydrothermal method was employed to synthesize Cu^{2+} exchanged SSZ-13 catalysts,[113] which was helpful to obtain the target products with small size, superior activity and adjustable crystal orientation. The temperature and time of the microwave synthesis were critical factors in determining the nucleation and growth process of SSZ-13. The optimal Cu-SSZ-13 zeolites were successfully prepared at the temperature of 175 °C and a synthesis time of 9 hours, resulting in more stable Al–O–Si structures of framework, larger specific surface area, and increased Cu^{2+} isolated species, thereby promoting the de-NO_x performance and hydrothermal stability (Fig. 8b).

Besides, a number of Fe-Cu-ZSM-5 zeolites synthesized through solid-state ion-exchanged (Fe-Cu-Z-SS), aqueous ion-exchanged (Fe-Cu-Z-AQ) and impregnation methods (Fe-Cu-Z-IM) were studied to investigate the impact of preparation methods on catalytic performance in NH_3-SCR.[114] The higher metal contents were reserved over Fe-Cu-Z-SS and Fe-Cu-Z-IM catalysts, and the mass of metal was significantly lost during the aqueous ion-exchanged method. However, the metal loss would not cause a decrease of performance, because the reserved Cu and Fe species metals existed in a more highly dispersed form on the Fe-Cu-Z-AQ zeolites, avoiding the ammonia peroxidation. By contrast, Fe-Cu-Z-SS and Fe-Cu-Z-IM zeolites showed a decreased high-temperature activity because of the peroxidation of ammonia, resulting from the presence of aggregated oxides. Other preparation methods focused on Cu-exchanged zeolites (Cu/SAPO-34) using mechanical mixing (Cu/SAPO-34-M) and ball milling (Cu/SAPO-34-B) methods were also explored for NH_3-SCR performance.[115] Characterization results suggested that ball milling was a more appropriate approach for achieving superior activity as it increased the number of isolated Cu^{2+} species over Cu/SAPO-34-B catalysts, which was beneficial for the activation of NO_x and the formation of Lewis acid sites, simultaneously promoting the redox property of the catalysts.

Copper species, including isolated Cu^{2+} ions, Cu dimers and CuO_x clusters, coexisted on the Cu-based catalysts. It was an important means to adjust the physicochemical characteristics of Cu species through changing the pretreatment method in the process of catalyst synthesis. Compared with isolated Cu^{2+} ions, most studies reported that CuO_x clusters cannot contribute to the low-temperature de-NO_x activity, and might even decrease the performance at high temperatures. Therefore, the high-temperature hydrogen treatment was beneficial for the reduction of Cu dimers to isolated Cu ions, thus providing a promising avenue for improving the activity of Cu-exchanged

Table 3 Representative Cu-based catalysts prepared by various methods for the SCR reaction

Catalysts	Preparation method	Reaction conditions	NO conversion	Ref.
Cu-SSZ-13	Incipient wetness impregnation	[NO] = [NH_3] = 500 ppm, [O_2] = 5%, GHSV = 180 000 h^{-1}	>80% (~250–500 °C)	112
	Ion exchange		>80% (~250–600 °C)	
	Hydrothermal synthesis		>90% (~215–600 °C)	
Fe-Cu-ZSM-5	Solid-state ion-exchanged	[NO] = [NH_3] = 1000 ppm, [O_2] = 8%, [H_2O] = 3.5 vol%, GHSV = 333 h^{-1}	>50% (above 270 °C)	114
	Aqueous ion-exchanged		>50% (above 280 °C)	
	Impregnation method		>50% (above 265 °C)	
Cu-SAPO-34	Mechanical mixing	[NO] = [NH_3] = 500 ppm, [O_2] = 5%, GHSV = 200 000 h^{-1}	<60% (~100–500 °C)	115
	Ball mixing		>60% (~200–450 °C)	

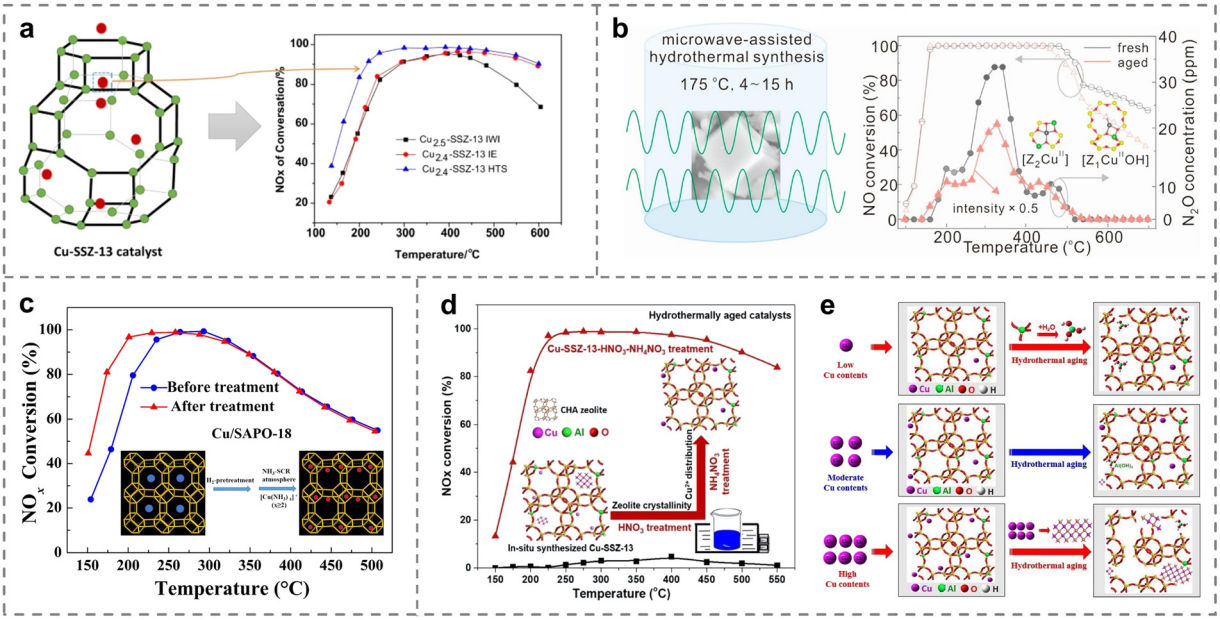

Fig. 8 (a) NH_3-SCR performance of various as-prepared catalysts with different preparation methods. Copied with permission from ref. 112. Copyright 2019, Springer Nature. (b) Microwave synthesis conditions and hydrothermal performance of the catalysts. Copied with permission from ref. 113. Copyright 2021, Elsevier. (c) NH_3-SCR activity of various Cu/SAPO-18 catalysts with different treatments. Copied with permission from ref. 116. Copyright 2019, Elsevier. (d) NH_3-SCR performance of various Cu-SSZ-13 zeolites with different treatments. (e) The deactivation mechanism of Cu-SSZ-13 with different Cu loadings during hydrothermal treatment. Copied with permission from ref. 117. Copyright 2020, Elsevier.

zeolites at low temperatures. Recent reports suggested that the low-temperature SCR activity would be related to the Cu^+/Cu^{2+} ratio. With the treatment of H_2 reduction, Cu^+ or $[Cu(OH)]^+$ species were formed by the reduction of Cu dimers and the Cu^+/Cu^{2+} ratio increased,[116] and then the resulting isolated Cu active sites exchanged into Cu-SAPO-18 catalysts. Notably, Cu ions would generate the mobile intermediates of ion-pairs after NH_3 solvation, promoting NO_x conversion at low temperatures (Fig. 8c). Another method was to pretreat the catalyst with HNO_3 and NH_4NO_3 to improve the performance of Cu-SSZ-13 zeolites in NH_3-SCR through adjusting the distribution and electronic properties of active Cu ions. Shan *et al.* firstly synthesized Cu-SSZ-13 zeolites with the treatment of HNO_3 and NH_4NO_3, employing Cu-TEPA as the template, achieving above 90% NO_x removal (250–450 °C), even after hydrothermal aging at 750 and 800 °C (Fig. 8d).[117] The optimal Cu/Al ratios (from 0.22 to 0.31) on the Cu-SSZ-13 zeolites was revealed to inhibit the dealumination of catalysts and the generation of CuO_x clusters, leading to the superior activity and hydrothermal stability. However, excessive amounts of Cu^{2+} species were easily transferred to form CuO_x clusters, leading to the destruction of the framework structure (Fig. 8e).

2.6 Interaction and interface engineering

The performance of SCR catalysts would be greatly modified by the combination of Cu-based catalysts with other materials owing to the regulation of interaction and interface. The interaction and interface engineering could give full play to the advantages of different components, influence the bonding and electron transfer at the atomic level, so as to optimize the adsorption and activation of gas molecules.[118,119] To improve the catalytic activity and hydrothermal stability of Cu-SSZ-13, Wei *et al.* designed core–shell catalysts with interconnected honeycomb structures by 3D printing strategies, in which the hydrophilic noncompact SiO_2 acted as shells and Cu-SSZ-13 zeolites served as cores (Fig. 9a).[120] In contrast, since pure Cu-SSZ-13 zeolites were limited by the interfacial diffusion, the interaction between SiO_2 shells and Cu-SSZ-13 cores increased the accessibility of Cu active centers on Cu-SSZ-13@SiO_2 (Fig. 9b), leading to superior de-NO_x performance (Fig. 9c). Notably, the thicker SiO_2 shells further promoted hydrothermal stability because of the inhibition of the dealumination process and the generation of CuO_x during the hydrothermal treatment (Fig. 9c and d). Similar observations were reported by Qu *et al.*, where the introduction of $BaMnO_3$ perovskite to mesoporous Cu-SSZ-13 generated small-scale nanocrystals (5–10 nm).[121] The doping of $BaMnO_3$ accelerated its synergistic effect with Cu ions thus leading to a higher Mn^{4+} proportion and stronger redox capacity on $BaMnO_3$-Cu-SSZ-13 catalysts, promoting the adsorption and activation of reactant gas molecules based on *in situ* DRIFT spectra. Moreover, the low-temperature performance was revealed to be enhanced by the interaction between Cu-SSZ-13 and doped $Ce_{0.7}Mn_{0.3}O_x$ oxides.[122] The reason was that HONO and N_2O_3 intermediates were firstly formed on the surface of the oxide phase, and then the intermediates could transfer and react with Brønsted acid sites of Cu-SSZ-13 zeolites (Fig. 9e).

Recently, lots of effort has been focused on the hybrid zeolites for enhancing NH_3-SCR reaction, and utilizing the interfacial interactions between different components was proved to be effective in promoting the catalytic activity. It is well known that Cu-SAPO-34 (Cu-CZC) catalysts show higher

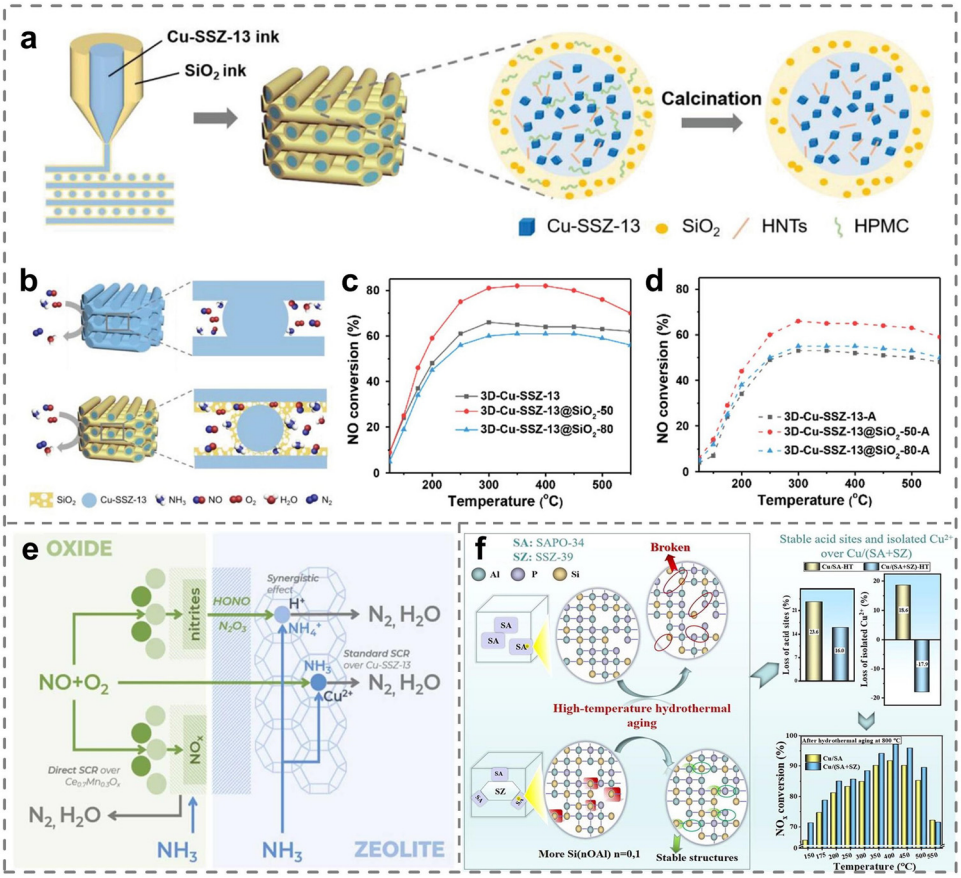

Fig. 9 (a) The preparation process of 3D-printed materials. (b) Schematic illustration of the diffusion of reactant/product gas over the catalysts in catalytic reaction. (c) and (d) NH_3-SCR performance of (c) fresh and (d) aged 3D-printed catalysts with various shell thicknesses. Copied with permission from ref. 120. Copyright 2023, Wiley. (e) The mechanism of enhanced catalytic activity of composite catalysts. Copied with permission from ref. 122. Copyright 2023, Elsevier. (f) Schematic diagram of Cu_2O/CuO interaction in the NH_3-SCR reaction. Copied with permission from ref. 124. Copyright 2020, Elsevier.

NO_x removal at lower temperatures (<300 °C) and Fe-Mordenite (Fe-MOR) is beneficial for eliminating NO_x at higher temperatures (>350 °C).[123] Based on this case, the mechanical mixture of the same amount of Cu-CZC and Fe-MOR was investigated to improve activity over a broad temperature range. Compared with the catalysts prepared with only one metal (Cu-CZC or Fe-MOR), the resulting mechanical mixture exhibited a larger number of acid sites, favorable redox properties, and higher NH_3-SCR performance when exposing to excess ammonia (NH_3/NO_x = 1.3). Moreover, stable SSZ-39 seeds were introduced to the precursors of SAPO-34 to synthesize the composite structure of SAPO-34 + SSZ-39 materials (SA + SZ).[124] With the modification of SSZ-39 zeolites, the interface of the Cu/(SA + SZ) samples induced higher contents of stable Si(*n*OAl) (*n* = 0, 1) structures and acid sites, accompanied by the formation of more Cu isolated species (Fig. 9f). To a certain degree, these enhancements of physical and chemical properties on Cu/(SA + SZ) samples was confirmed to be beneficial for achieving better activity and hydrothermal stability compared to Cu/SA. Generally, it was well-known that the SCR performance of highly dispersed Cu cations demonstrated satisfactory performance in the catalytic process, but the influence of the electronic properties of Cu species on NH_3-SCR reactions remained unclear. In this case, the electron transfer between Cu^+ and Cu^{2+} had been widely explored with interfacial engineering by constructing composite materials. CuAl-LDO/CNTs catalysts with the controllable valence states of Cu ions were prepared by combining CuAl-layered double oxide and various mass fractions of carbon nanotubes,[125] revealing the synergistic effect between Cu_2O and CuO at the atomic level. The results demonstrated that the CuO species were used for the adsorption of NO and NH_3, which was beneficial to activate NH_3 molecules and promote the generation of NO^+ species. Meanwhile, the Cu_2O centers served as active sites for adsorbing O species, thereby enhancing the generation of active O^- species. Therefore, the flexible and adjustable structure of Cu-based catalysts enabled them to from rich interfaces with other materials, and optimized the structure–activity relationship of the composite materials, resulting in the enhancement of the catalytic performance.

3. The reaction mechanism and strategies for enhanced poisoning-resistant and hydrothermal stability

As we all know, SO_2 and alkali metals exist in real flue gas, which could directly or indirectly affect the active centers of Cu-

based SCR catalysts, leading to the deactivation of de-NO_x catalysts.[126–128] For SCR catalysts, they were positioned in close proximity to the diesel particulate filter and were exposed to a temperature above 650 °C, thereby experiencing hash hydrothermal aging conditions during practical use. Therefore, it was important to investigate the effect of SO_2 and alkali metals and to design Cu-based catalysts with superior resistance and hydrothermal stability for the NH_3-SCR catalytic process. In this part, we provide a comprehensive summary of the catalyst deactivation mechanisms caused by these components and propose several viable strategies.

3.1 SO_2 poisoning-resistance

Inevitably, even low levels of SO_2 from ultra-low sulfur fuel could deactivate catalysts under practical conditions, posing limitations on the development of Cu-based catalysts.[129–132] SO_2 molecules reacted with NH_3 and H_2O at appropriate temperatures to form ammonium bisulfate, which further reacted with catalyst components to generate metal sulfates. Generally, low temperature and high concentrations of SO_2 would accelerate the deposition of ammonium sulfate on the surface of catalysts, thus reducing the denitrification efficiency. The generation of metal sulfates would fill micropores of catalysts, causing a decrease in specific surface area and pore volume, which hindered the adsorption and activation of gas reactants.[133,134] To address this issue, Wang *et al.* employed acidic $NbOPO_4$ species to mitigate the SO_2 poisoning effect of mixed CuCe oxides.[135] The strong interaction between $NbOPO_4$ and CuCe mixed oxides restrained the oxidation process of interfacial oxygen atoms and SO_2, thus exhibiting superior NO conversion on CuCe/Nb-P samples when exposed to the conditions of SO_2 (100 ppm) and H_2O (5 vol%) for 10 hours. Additionally, the CuZ-Ce_n catalysts modified with the thin CeO_2 film were prepared using liquid deposition, and the

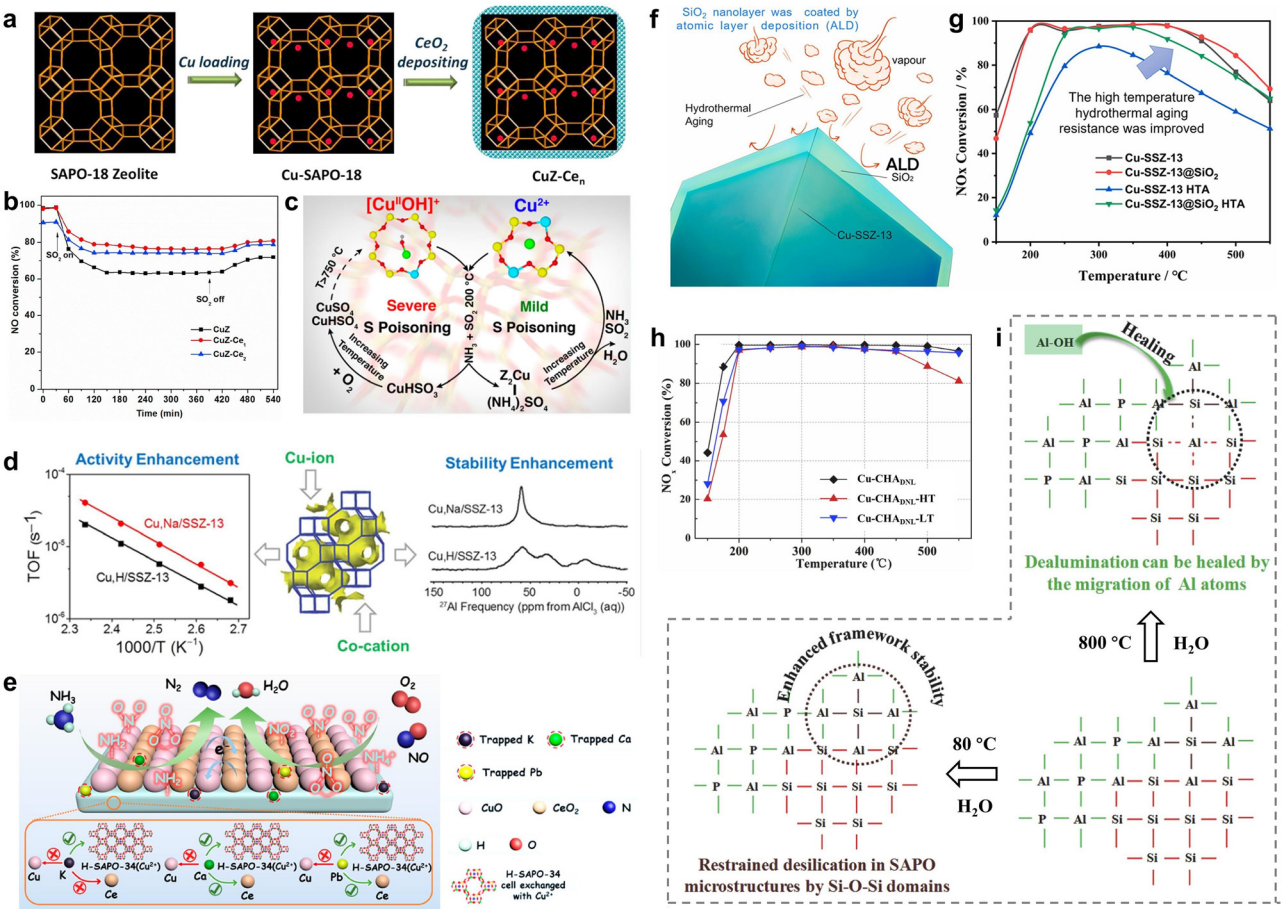

Fig. 10 (a) The schematic diagram for the synthesis of CuZ-Ce_n catalysts. (b) NH_3-SCR performance of as-prepared catalysts with the exposure of 100 ppm SO_2. Copied with permission from ref. 69. Copyright 2017, Elsevier. (c) Proposed formation of sulphates during adsorption of SO_2 on $[Cu(OH)]^+$–Al and Cu^{2+}–2Al sites. Copied with permission from ref. 137. Copyright 2017, American Chemical Society. (d) The activity enhancement and stability enhancement on Cu-SSZ-13 by co-cations. Copied with permission from ref. 144. Copyright 2015, American Chemical Society. (e) Schematic diagram of enhanced alkaline-resistance and heavy metal-resistance on CuCe/H-SAPO-34. Copied with permission from ref. 147. Copyright 2020, American Chemical Society. (f) The protection mechanism of the ALD effect of SiO_2. (g) NH_3-SCR performance of the as-prepared catalysts. Copied with permission from ref. 156. Copyright 2021, Elsevier. (h) NH_3-SCR performance on Cu-CHA_{DNL} catalysts before (black) and after hydrothermal treatment (HT: red; LT: blue). (i) Proposed mechanism for the enhanced hydrothermal stability over Cu-CHA_{DNL} catalysts at high and low temperatures. Copied with permission from ref. 157. Copyright 2020, Elsevier.

protective effect of the CeO_2 thin film was revealed to promote the resistance to H_2O and SO_2 on Cu-SAPO-18 (Fig. 10a).[69] The enhancement of H_2O-resistant ability was attributed to the fact that CeO_2 inhibited the aggregation of isolated Cu^{2+} species into Cu clusters and inhibited the infection of H_2O molecules on Cu active species and acid centers. Meanwhile, the presence of thin CeO_2 film restrained the generation and deposition of sulfates, thus preventing the blocking of active centers over CuZ-Ce_n catalysts and resulting in higher resistance to SO_2 compared to Cu-SAPO-18 (Fig. 10b).

Moreover, from the studies of Chen *et al.*, three Cu^{2+} active sites (named Cu_1, Cu_2 and Cu_3) were identified to occupy different positions of I, III and IV on Cu-SSZ-13, respectively.[136] Cu_1 species were located near the window of the eight-membered rings, Cu_2 species were positioned in the super cage deviated from the double six-membered rings, and Cu_3 species were present at the center of the hexagonal prism. Among them, the content of Cu_2 (1.81%) was higher than that of Cu_1 (0.98%) and Cu_3 (0.46%). The results demonstrated that Cu_1 species played a crucial role in enhancing the performance of catalysts at low temperatures, and Cu_3 species contributed to the excellent SO_2 resistance because of the high stability. Notably, Jangjou *et al.* carried out a study on the impact of SO_2 on two types of active Cu species (Cu^{2+}–2Al and $[Cu(OH)]^+$–Al) over Cu-SSZ-13 catalysts.[137] From this research, the activity of both active Cu sites for low-temperature SCR functionality was significantly inhibited by SO_2, but their behavior of desulfation differed. Compared to the Cu^{2+}-2Al structure, ZCuOH species were more likely to suffer severe SO_2 poisoning at low temperatures, as it led to the blocking of active sites by the generation of unbreakable bisulfite and bisulfate products. This finding suggested that Cu-SSZ-13 with a larger number of $[Cu(OH)]^+$–Al components required higher desulfation temperatures (above 550 °C) (Fig. 10c). To promote the service life and SO_2 resistance of the catalysts, efforts have been made to prevent the sulfation of active sites. Previous studies have focused on the enhancement of SO_2-resistance on SCR catalysts through the incorporation of individual components. For instance, hybrid catalysts combining Cu-SSZ-13 zeolite with metal oxides (Mn, Co, Ni, and Zn) demonstrated excellent SO_2 resistance compared to pure Cu-SSZ-13 zeolites.[138] Among them, the addition of $ZnTi_{10}O_x$ had the most significant effect on improving performance by acting as the sacrificial component that reacted with SO_2, thereby protecting Cu^{2+} from sulfur deactivation. Similarly, yttrium-modified Cu-SSZ-39 also exhibited significantly higher NO_x conversion after exposure to SO_2,[139] and the reason was that the doping of Y species stabilized Cu^{2+} species from six-membered rings and reduced the sensitivity of the reaction between Cu^{2+} and SO_2. These strategies provided a general and straightforward approach to decrease the sensitivity of active centers towards SO_2 in catalytic processes. Except for the Cu-based small-pore zeolites, the design of Cu_yAlO_x mixed oxide materials derived from Cu–Al LDHs precursors was confirmed to have a superior SO_2 resistance compared with CuO/γ-Al_2O_3. And the enhancement of tolerant ability for poisoning might be attributed to the presence of highly dispersed CuO nanoparticles, which induced that the acidic sites and redox property remained and were less influenced by the poisoning of SO_2.[140] Another similar catalyst with the chemical composition of $Cu_wMn_yTi_{1-y}O_x$ showed significant resistance to 100 ppm SO_2 after copper oxides was introduced, which was associated with the excellent surface acidity and the generation of more MnO_2 and CuO species, indicating the greater potential for industrial applications.[141]

3.2 Alkali metal poisoning-resistance

Alkali metal ions mainly originated from the flue gas or aerosol particles of glass furnaces, biomass power generation and urea solutions, would deposit on catalysts and strongly affect their catalytic activity.[142,143] However, the effect of alkali metals on Cu-based catalysts has not been well understood. Gao *et al.* demonstrated that co-cations helped reduce the hydrolysis of Cu-SSZ-13 zeolites in the hydrothermal treatment, as evidenced by ^{27}Al NMR. In particular, Li^+ and Na^+ ions significantly promoted the rate of SCR at low temperatures (Fig. 10d).[144] Nevertheless, several studies have shown that alkali metal ions would volatilize and diffuse to the catalyst surface at high temperatures, resulting in catalyst poisoning. Fundamental research has revealed the mechanisms of alkali metal poisoning on Cu-based catalysts, indicating that the deactivation might be attributed to the pore blockage or damage to the acidic and redox sites caused by alkali metal impurities. From systematic research, Fan *et al.* explored the influence of alkali metal and alkaline earth metals (Na^+, K^+, Mg^{2+} and Ca^{2+}) on the catalytic performance of Cu-SSZ-13 zeolites.[145] The results showed that the introduction of Mg and Ca caused more serious destruction to the framework structures, resulting in the replacement of more isolated Cu^{2+} species and the formation of extra-framework CuO_x clusters. For Cu-SSZ-39 zeolites, the toxicity degree of alkali and alkaline earth metals to catalyst deactivation was K > Mg > Ca > Na.[146] The presence of the above impurities (at a concentration of 1 mmol per gram of catalyst) significantly decreased the specific surface area, isolated Cu^{2+} species and acid centers of the catalysts after poisoning. Thus, the development of a novel catalyst with superior resistance to alkali and alkaline earth metal poisoning is of great concern for de-NO_x applications.

Based on the understanding of the deactivation mechanism, a potential method for designing alkali-resistant catalysts was to increase the number of active sites or develop sacrificial sites that could trap alkali metals. For instance, the H-SAPO-34 support, which possessed abundant acid centers, protected the activity of active copper components through reacting with alkali metals (K), alkaline earth metals (Ca) and heavy metals (Pb) (Fig. 10e). Furthermore, the introduction of Ce species enhanced the low-temperature performance by facilitating the redox process with Cu active centers and assisting H-SAPO-34 to capture Pb and Ca impurities, resulting in excellent de-NO_x performance and resistance against the alkaline metal and heavy metal on CuCe/H-SAPO-34 zeolites.[147] Similarly, Nb–OH and Nb=O structures were preferentially link to K atoms on CuNbTi oxides, which resulted in more active Cu species being

protected and the weak acid sites were preserved, contributing the superior alkali metal resistance.[148] And Li *et al.* utilized the interaction of V, Ce and Cu species to develop excellent alkali metal poisoning-resistant VWCeCuTi catalysts, and the results suggested that the addition of Cu species would increase the acidic sites and improve the redox property, which contributed to the superior K resistance.[149] Besides, the construction of the core–shell structure was confirmed to have practical value.[150] By increasing the crystalline sizes of SSZ-13, the active Cu species were regulated to be located in the subsurface or inner core, thereby buffering alkali metal poisoning on the outer layer of zeolites. The dispersion of acid centers could be adjusted through changing the crystalline sizes, which provided a simple and easy approach to enhance performance against alkali metals.

3.3 Hydrothermal stability

Cu-Based SCR catalysts, particularly small-pore zeolites, were prone to hydrothermal aging and deactivation when exposed to the harsh tail gas atmosphere in real applications.[151–153] This led to the efflux of alumina to the surface of the catalysts at high temperature. The deactivation would be relevant to the aggregation of Cu^{2+} ions into CuO_x oxide species or dealumination occurring in Cu-based small-pore zeolites upon exposure to the tail gas.[154,155] These findings highlighted the need to efficiently promote hydrothermal stability of de-NO_x catalysts at high temperatures. From the destruction mechanism, utilizing the Al-rich support for stabilizing Cu species is effective to promote hydrothermal stability. Moreover, Tian *et al.* successfully enhanced the catalytic activity of NO_x reduction through using the atomic layer deposition (ALD) approach to coat the surface of Cu-SSZ-13 catalysts with SiO_2 nanolayers (Fig. 10f).[156] The integrity of the Cu-SSZ-13 framework was well preserved even after 16 hours of hydrothermal treatment at 800 °C with 12.5 vol% H_2O, owing to the protection of SiO_2 layers. The layers effectively slowed down the formation of CuO clusters by inhibiting the accumulation of Cu and stabilizing the positions of Cu^{2+} ions in the zeolite frameworks by suppressing dealumination, thereby promoting the hydrothermal aging resistance of the Cu-SSZ-13@SiO_2 HTA catalysts (Fig. 10g).

Moreover, there was evidence supporting the notion that the preparation of zeolite–zeolite composites would effectively promote high-temperature hydrothermal stability. It was acknowledged that Cu-SSZ-13 was prone to dealumination and deactivation after hydrothermal aging at high temperatures. Conversely, SAPO-34 zeolites exhibited irreversible framework degradation during repeated ion-exchange (Cu species) processes or exposure to low-temperature moisture atmospheres, which was avoided in the case of SSZ-13 zeolites. Thus, it was highly desirable to design Cu-based composites that combined the advantages of both Cu-SAPO-34 and Cu-SSZ-13. Sun *et al.* synthesized novel Cu-CHA composites (Cu-CHA_{DNL}) by interlacing SAPO and aluminosilicate parts, utilizing Cu-SSZ-13 as the compounds to promote the crystallization of SAPO-34.[157] As displayed in Fig. 10i, the Si–O–Al framework of SAPO was closely linked to Si–O–Si structures in aluminosilicate, resulting in increased difficulty of desilication in the SAPO part. This effectively restrained framework degradation over Cu-CHA_{DNL} catalysts when exposed to H_2O. Meanwhile, adjacent Al–O–P groups facilitated the healing of dealumination in the aluminosilicate parts through migration to defects at high temperatures, thereby promoting high-temperature hydrothermal stabilities. In this work, the high-temperature hydrothermal treatment was carried out at 800 °C for 16 hours, which contained 10 vol% water, and the low-temperature hydrothermal treatment was performed through immersing the catalyst at 80 °C deionized water for 24 hours in a closed vessel. Consequently, Cu-CHA_{DNL} compounds with the microstructural properties of both Cu-SSZ-13 and Cu-SAPO-34 demonstrated excellent catalytic activity and robust high-temperature and low-temperature hydrothermal stability (Fig. 10h). Additionally, mechanically mixed samples containing Cu-SSZ-13 and Cu-SAPO-34 zeolites were found to significantly improve hydrothermal stability compared to single-component catalysts. Ma *et al.* proposed that the strong interaction between Cu-SAPO-34 and Cu-SSZ-13 was beneficial in suppressing the dealumination of SSZ-13 and preserving framework structures.[158] Thereafter, the migration of extra-framework P atoms in SAPO-34 would occupy Al atoms in the fragmented SSZ-13 framework, inhibiting further damage of the Si–O–Al structure in hydrothermal treatments. Therefore, synthesizing zeolite–zeolite composites through two-phase intergrowth is of great significance, as it aims to leverage the advantages of individual zeolites while harnessing specific synergistic properties.

4. Conclusions

4.1 Summary

NH_3-SCR reaction will effectively remove NO_x and convert them into the harmless gases, which is of great significance to environmental protection and has high application value. Herein, we present an in-depth overview of the latest advancements in catalytic reaction mechanisms over Cu-based SCR catalysts (including Cu-based small-pore zeolites and Cu-containing metal oxides). Meanwhile, the review gives a valuable summary of new insights about the essence of NH_3-SCR catalytic reaction and the design strategies of Cu-based catalysts, and then efficient solutions against harmful components encountered in real applications are further proposed. This is helpful to provide insights into catalytic mechanisms on various catalysts in the NH_3-SCR reaction, thereby facilitating the development of highly active and resistance-enhanced catalysts to deal with complex environmental problems by designing reasonable modification strategies.

Based on the mechanism of the NH_3-SCR reaction, the adsorption and activation of NH_3 and NO molecules are the initial and crucial steps in the catalytic process. In this regard, both excellent redox properties and strong acidity are important factors that contribute to the activity enhancement of SCR catalysts. The reason is that the enhanced redox performance will be beneficial to the activation of NO gas at the active centers, thus promoting the catalytic activity of the catalysts

at low temperature. Besides, abundant strong acid centers help to enhance the activation of NH_3 molecules, forming NH_3 (Lewis acid sites) and NH_4^+ (Brønsted acid sites) species, which will react with active nitrate and nitrite intermediates formed by NO activation in the subsequent reaction. For efficient NO_x removal, one feasible design is introducing components which have excellent redox properties such as Ce, Nb or Zr for the oxidation of NO molecules, combined with acid components including W, Mo or zeolites providing adsorption sites to improve the activation of NH_3 molecules, thus accelerating the NH_3-SCR process.

Recently, Cu-based SCR catalysts (Cu-based small-pore zeolites and Cu-containing metal oxides) have been rapidly developed in the field of NH_3-SCR, but their further application is limited due to their own shortcomings. Cu-based small-pore zeolites always have better catalytic performance at low temperatures, while their high-temperature activity and hydrothermal stability are not satisfactory. In addition, due to the high price of Cu-based small-pore zeolites, the development of Cu-containing metal oxides is of great significance. The main challenge of these catalysts is that their operating temperature window is too narrow. In this case, improving the temperature window will be an important research direction in the future. Therefore, a large number of optimization studies have been carried out on the design and development of Cu-based catalysts, aiming to explore novel Cu-based small-pore zeolites and Cu-containing metal oxides through common modifications of the catalyst structure and active sites, so as to achieve higher activity and hydrothermal stability.

Specifically speaking, there are great differences in specific active sites and redox routeways in NH_3-SCR reaction catalysed by various systems of Cu-based catalysts, which leads to the complexity of the reaction mechanism. Therefore, it is meaningful to develop catalysts with a specific reaction path to optimize the reaction kinetics and facilitate the NH_3-SCR process from the perspective of catalyst design, further promoting the reaction activity of Cu-based catalysts. Firstly, due to the different physicochemical properties and specific surface area, the supports had different effects on the chemical valence states and dispersion of Cu active species, so selecting an appropriate support and in-depth understanding of the reaction mechanism have guiding significance to enhance catalysis. Secondly, the growth of the zeolite framework, and the number and location of active Cu species play an important role in the catalytic performance, redox and acid ability of the catalysts. Controllable regulation will be achieved through strategies including precursor optimization engineering and preparation method modification, which can also induce the generation of more isolated Cu ions and promote the adsorption/activation of reactant gas molecules on the catalyst surface. Moreover, the structure–activity relationship needs to be further revealed. Crystal structure regulation, secondary metal doping (Fe, Ce, Y, *etc.*), and interaction and interface engineering (the composite between molecular sieves, the composite between molecular sieve and metal oxides, *etc.*), directly affecting the redox/acid properties of the catalysts and accelerating the electron transfer between foreign components and active Cu species, will be efficient strategies to design high-performance Cu-based catalysts.

Although great efforts have been made in the design and development of Cu-based SCR catalysts, there are still many serious challenges in industrial applications. Due to the complex composition of flue gas, the chemical poisoning resistance (SO_2 and alkali metals *etc.*) and hydrothermal resistance for NH_3-SCR catalysts should be enhanced. An efficient strategy to promote SO_2-resistance is to optimize the redox property of the catalysts, which will weaken the oxidation of SO_2 on the catalyst surface and promote the decomposition of ammonium bisulfate. To avoid the poisoning of alkali ions, choosing strongly acidic supports or metals should be effective, which will interact with alkali ions and reduce the poisoning effect of alkali metals on the active sites. For Cu-based small-pore zeolites, the generation of CuO_x induces dealumination and collapse of the zeolite framework during hydrothermal aging. In this case, constructing a stable structure of the zeolite framework, and utilizing an Al-rich support for stabilizing Cu species is necessary to promote hydrothermal stability. Notably, the addition of other components to design composite materials with separated catalytically active sites and sacrificial centers should be a universal way to increase the hydrothermal stability and resistance to SO_2 and alkali metals, which is helpful to realize the industrial application of Cu-based catalysts.

4.2 Future perspectives

As summarized above, selective catalytic reduction of NO_x with ammonia constitutes a vital component within the complicated aftertreatment system for flue gas removal. This process encompasses the efficient adsorption and activation of NO and NH_3 molecules, as well as the precise formation and transfer of various intermediates. Therefore, acting as the widely used de-NO_x catalyst, the optimization of the catalyst structure and active centers of Cu-based catalysts significantly impacts the regulation of catalytic activity. Meanwhile, the exploration of catalyst synthesis and preparation at the atomic scale plays a pivotal role in practical production. However, there remains a need for a deeper understanding of fundamental mechanisms governing interactions among various active components, particularly under realistic reaction conditions, which poses a challenge to further catalyst optimization. Therefore, achieving a comprehensive understanding of the interplay between active components holds immense importance for enhancing the reliability and long-term economic viability of catalyst design and processes. Moreover, to advance the industrialization of Cu-based catalysts, superior resistance to toxicity is imperative, given the presence of numerous toxic constituents in industrial production processes. Subtle adjustments to the catalyst structure and active sites or alterations in reaction pathways can mitigate the combination of active sites with harmful components under the complex flue gas environment, which is of paramount significance for future practical applications. Consequently, the optimization of catalysts and processes to attain outstanding activity and toxicity-resistance represents a foremost research direction, offering promising prospects in future industrial production.

Conflicts of interest

The authors declare no competing interests.

Acknowledgements

The authors gratefully acknowledge the financial support by the National Science Foundation of China (grant No. 22225604, 22076082 and 22176140), the Frontiers Science Center for New Organic Matter (grant No. 63181206), and the Haihe Laboratory of Sustainable Chemical Transformations.

Notes and references

1 S. Xie, W. Tan, Y. Li, L. Ma, S. N. Ehrlich, J. Deng, P. Xu, F. Gao, L. Dong and F. Liu, *ACS Catal.*, 2022, **12**, 2441–2453.
2 C. Kim, G. Qi, K. Dahlberg and W. Li, *Science*, 2010, **327**, 1624.
3 M. V. Twigg, *Appl. Catal., B*, 2007, **70**, 2–15.
4 S. C. Anenberg, J. Miller, R. Minjares, L. Du, D. K. Henze, F. Lacey, C. S. Malley, L. Emberson, V. Franco, Z. Klimont and C. Heyes, *Nature*, 2017, **545**, 467–471.
5 F. H. Johnston, N. Borchers-Arriagada, G. G. Morgan, B. Jalaludin, A. J. Palmer, G. J. Williamson and D. M. J. S. Bowman, *Nat. Sustainability*, 2020, **4**, 42–47.
6 A. Richter, J. P. Burrows, H. Nuss, C. Granier and U. Niemeier, *Nature*, 2005, **437**, 129–132.
7 D. R. Kanter, O. Chodos, O. Nordland, M. Rutigliano and W. Winiwarter, *Nat. Sustainability*, 2020, **3**, 956–963.
8 C. Oberschelp, S. Pfister, C. E. Raptis and S. Hellweg, *Nat. Sustainability*, 2019, **2**, 113–121.
9 R. Zhang, N. Liu, Z. Lei and B. Chen, *Chem. Rev.*, 2016, **116**, 3658–3721.
10 H. He, Y. Wang, Q. Ma, J. Ma, B. Chu, D. Ji, G. Tang, C. Liu, H. Zhang and J. Hao, *Sci. Rep.*, 2014, **4**, 4172.
11 A. Skowron, D. S. Lee, R. R. De Leon, L. L. Lim and B. Owen, *Nat. Commun.*, 2021, **12**, 564.
12 M. Gao, Z. Li, G. He, Y. Shan, Y. Sun and H. He, *Environ. Sci. Technol.*, 2023, **57**, 8426–8434.
13 Z. Shen, A. Chen, Y. Shen, X. Liu, Q. Yi, P. Wang, K. Zhang and D. Zhang, *Fuel*, 2023, **349**, 128655.
14 P. Wang, G. Liu, Z. Hao, H. Zhang, Y. Li, W. Sun, L. Zheng and S. Zhan, *Proc. Natl. Acad. Sci. U. S. A.*, 2023, **120**, e2216584120.
15 P. S. Kim, M. K. Kim, B. K. Cho, I.-S. Nam and S. H. Oh, *J. Catal.*, 2013, **301**, 65–76.
16 S. Zinatloo-Ajabshir, N. Ghasemian, M. Mousavi-Kamazani and M. Salavati-Niasari, *Ultrason. Sonochem.*, 2021, **71**, 105376.
17 S. Zinatloo-Ajabshir, N. Ghasemian and M. Salavati-Niasari, *Ceram. Int.*, 2020, **46**, 66–73.
18 Y. Wang, J. Han, M. Chen, W. Lv, P. Meng, W. Gao, X. Meng, W. Fan, J. Xu, W. Yan and J. Yu, *Angew. Chem., Int. Ed.*, 2023, e202306174.
19 Y. Wei, S. Wang, M. Chen, J. Han, G. Yang, Q. Wang, J. Di, H. Li, W. Wu and J. Yu, *Adv. Mater.*, 2023, e2302912.
20 Y. Long, Y. Su, M. Chen, S. Lu, X. Luo, Z. Zhu, Z. Wu and X. Weng, *Environ. Sci. Technol.*, 2023, **57**, 7590–7598.
21 Y. Wu, W. Zhao, S. H. Ahn, Y. Wang, E. D. Walter, Y. Chen, M. A. Derewinski, N. M. Washton, K. G. Rappe, Y. Wang, D. Mei, S. B. Hong and F. Gao, *Nat. Commun.*, 2023, **14**, 2633.
22 S. Han, W. Rao, J. Hu, X. Tang, Y. Ma, J. Du, Z. Liu, Q. Wu, Y. Ma, X. Meng, W. Shan, F.-S. Xiao and H. He, *Appl. Catal., B*, 2023, **332**, 122746.
23 Y. Shan, J. Du, Y. Zhang, W. Shan, X. Shi, Y. Yu, R. Zhang, X. Meng, F. S. Xiao and H. He, *Natl. Sci. Rev.*, 2021, **8**, 134–153.
24 J. Liu, H. Cheng, H. Zheng, L. Zhang, B. Liu, W. Song, J. Liu, W. Zhu, H. Li and Z. Zhao, *ACS Catal.*, 2021, **11**, 14727–14739.
25 G. Xu, X. Guo, X. Cheng, J. Yu and B. Fang, *Nanoscale*, 2021, **13**, 7052–7080.
26 L. Han, S. Cai, M. Gao, J. Y. Hasegawa, P. Wang, J. Zhang, L. Shi and D. Zhang, *Chem. Rev.*, 2019, **119**, 10916–10976.
27 J. Zhang, L. Chen, Y. Fan, C. Zhao, W. Dai, L. Yang, L. Zhou, J. Zou and X. Luo, *Chem. Eng. J.*, 2023, **465**, 142759.
28 H. Liu, C. Gao, J. Chen, J. Mi, S. Yang, D. Chen, W. Si, Y. Peng, C. Sun and J. Li, *Appl. Catal., B*, 2023, **332**, 122651.
29 K. Song, K. Guo, S. Mao, D. Ma, Y. Lv, C. He, H. Wang, Y. Cheng and J.-W. Shi, *ACS Catal.*, 2023, **13**, 5020–5032.
30 C. Tang, H. Zhang and L. Dong, *Catal. Sci. Technol.*, 2016, **6**, 1248–1264.
31 L. Lietti, J. L. Alemany, P. Forzatti, G. Busca, G. Ramis, E. Giamello and F. Bregani, *Catal. Today*, 1996, **29**, 143–148.
32 N. Topsøe, J. Dumesic and H. Topsøe, *J. Catal.*, 1995, **151**, 241–252.
33 N. Topsøe, H. Topsøe and J. Dumesic, *J. Catal.*, 1994, **151**, 226–240.
34 M. Rezayeenik, M. Mousavi-Kamazani and S. Zinatloo-Ajabshir, *Appl. Phys. A: Mater.*, 2023, **129**, 47.
35 S. Zinatloo-Ajabshir, S. Mortazavi-Derazkola and M. Salavati-Niasari, *J. Mol. Liq.*, 2017, **231**, 306–313.
36 S. Zinatloo-Ajabshir and M. Mousavi-Kamazani, *Ceram. Int.*, 2021, **47**, 23702–23724.
37 A. Cai, H. He, Q. Zhang, Y. Xu, X. Li, F. Zhang, B. Fan, W. Peng and Y. Li, *ACS Appl. Mater. Interfaces*, 2021, **13**, 13087–13096.
38 S. Yue, P. Wang, B. Yu, T. Zhang, Z. Zhao, Y. Li and S. Zhan, *Adv. Energy Mater.*, 2023, 2302008.
39 S. M. Tabatabaeinejad, S. Zinatloo-Ajabshir, O. Amiri and M. Salavati-Niasari, *RSC Adv.*, 2021, **11**, 40100.
40 S. Zinatloo-Ajabshir, M. S. Morassaei and M. Salavati-Niasari, *Composites, Part B*, 2019, **167**, 643–653.
41 J. Lin, X. Hu, Y. Li, W. Shan, X. Tan and H. He, *Appl. Catal., B*, 2023, **331**, 122705.
42 H. Liu, F. Gao, S. Ko, N. Luo, X. Tang, H. Yi and Y. Zhou, *Appl. Catal., B*, 2023, **330**, 122742.
43 Z. Huang, S. Guo, W. Chen, M. Huang, J. Ni, Q. Zhou, M. Tian, X. Wu, H. Zhao, H. Shen, W. Li and G. Jing, *Chem. Eng. J.*, 2023, **464**, 142540.

44 X. Tan, S. Zhang and S. B. Hong, *Appl. Catal., B*, 2023, **329**, 122552.
45 X. Huang, F. Dong, G. Zhang and Z. Tang, *J. Catal.*, 2023, **420**, 134–150.
46 F. Beshkar, S. Zinatloo-Ajabshir and M. Salavati-Niasari, *Chem. Eng. J.*, 2015, **279**, 605–614.
47 S. Zinatloo-Ajabshir and M. Salavati-Niasari, *Composites, Part B*, 2019, **174**, 106930.
48 S. Zinatloo-Ajabshir and M. Salavati-Niasari, *J. Mol. Liq.*, 2016, **216**, 545–551.
49 S. Zinatloo-Ajabshir and M. Salavati-Niasari, *New J. Chem.*, 2015, **39**, 3948.
50 I. Nova, L. Acqua, L. Lietti, E. Giamello and P. Forzatti, *Appl. Catal., B*, 2001, **35**, 31–42.
51 Z. Hao, G. Liu, N. Ma, H. Zhang, Y. Li, Y. Xia, D. Zhang and S. Zhan, *J. Environ. Chem. Eng.*, 2021, **9**, 106024.
52 X. Wu, Z. Chen, X. Yu, Z. Huang, H. Shen and G. Jing, *Chem. Eng. J.*, 2020, **399**, 125629.
53 P. Zhang, P. Wang, S. Impeng, T. Lan, X. Liu and D. Zhang, *Environ. Sci. Technol.*, 2022, **56**, 12553–12562.
54 G. Liu, H. Zhang, P. Wang, Y. Li, X. Mi and S. Zhan, *Fuel*, 2024, **357**, 129816.
55 J. Liu, Y. Wei, P.-Z. Li, P. Zhang, W. Su, Y. Sun, R. Zou and Y. Zhao, *ACS Catal.*, 2018, **8**, 3865–3874.
56 X. Mou, B. Zhang, Y. Li, L. Yao, X. Wei, D. S. Su and W. Shen, *Angew. Chem., Int. Ed.*, 2012, **51**, 2989–2993.
57 Z. Shen, P. Wang, X. Hu, W. Qu, X. Liu and D. Zhang, *Environ. Sci. Technol.*, 2023, **57**, 14472–14481.
58 J. Zou, S. Impeng, F. Wang, T. Lan, L. Wang, P. Wang and D. Zhang, *Environ. Sci. Technol.*, 2022, **56**, 13368–13378.
59 Y. Zhao, L. Shi, Y. Shen, J. Zhou, Z. Jia, T. Yan, P. Wang and D. Zhang, *Environ. Sci. Technol.*, 2022, **56**, 4386–4395.
60 P. Chen, A. Khetan, M. Jabłońska, J. Simböck, M. Muhler, R. Palkovits, H. Pitsch and U. Simon, *Appl. Catal., B*, 2018, **237**, 263–272.
61 J. Du, Y. Shan, Y. Sun, M. Gao, Z. Liu, X. Shi, Y. Yu and H. He, *Appl. Catal., B*, 2021, **294**, 120237.
62 A. Oda, H. Shionoya, Y. Hotta, T. Takewaki, K. Sawabe and A. Satsuma, *ACS Catal.*, 2020, **10**, 12333–12339.
63 S. Ali, L. Chen, Z. Li, T. Zhang, R. Li, S. U. H. Bakhtiar, X. Leng, F. Yuan, X. Niu and Y. Zhu, *Appl. Catal., B*, 2018, **236**, 25–35.
64 J. Zhang, J. Liang, H. Peng, Y. Mi, P. Luo, H. Xu, M. He and P. Wu, *Appl. Catal., B*, 2021, **292**, 120163.
65 S. Zhang, L. Pang, Z. Chen, S. Ming, Y. Dong, Q. Liu, P. Liu, W. Cai and T. Li, *Appl. Catal., A*, 2020, **607**, 117855.
66 C. Negri, T. Selleri, E. Borfecchia, A. Martini, K. A. Lomachenko, T. V. W. Janssens, M. Cutini, S. Bordiga and G. Berlier, *J. Am. Chem. Soc.*, 2020, **142**, 15884–15896.
67 Y. Feng, T. V. W. Janssens, P. N. R. Vennestrøm, J. Jansson, M. Skoglundh and H. Grönbeck, *J. Phys. Chem. C*, 2021, **125**, 4595–4601.
68 A. Turrina, E. C. V. Eschenroeder, B. E. Bode, J. E. Collier, D. C. Apperley, P. A. Cox, J. L. Casci and P. A. Wright, *Microporous Mesoporous Mater.*, 2015, **215**, 154–167.
69 Y. Li, W. Song, J. Liu, Z. Zhao, M. Gao, Y. Wei, Q. Wang and J. Deng, *Chem. Eng. J.*, 2017, **330**, 926–935.
70 Y. Li, J. Deng, W. Song, J. Liu, Z. Zhao, M. Gao, Y. Wei and L. Zhao, *J. Phys. Chem. C*, 2016, **120**, 14669–14680.
71 M. Moreno-González, R. Millán, P. Concepción, T. Blasco and M. Boronat, *ACS Catal.*, 2019, **9**, 2725–2738.
72 A. Godiksen, F. N. Stappen, P. N. R. Vennestrøm, F. Giordanino, S. B. Rasmussen, L. F. Lundegaard and S. Mossin, *J. Phys. Chem. C*, 2014, **118**, 23126–23138.
73 C. Paolucci, I. Khurana, A. Parekh, S. Li, A. Shih, H. Li, J. Iorio, J. Albarracin-Caballero, A. Yezerets, J. Miller, W. Delgass, F. Ribeiro, W. Schneider and R. Gounder, *Science*, 2017, **357**, 898–903.
74 C. Paolucci, A. A. Parekh, I. Khurana, J. R. Di Iorio, H. Li, J. D. Albarracin Caballero, A. J. Shih, T. Anggara, W. N. Delgass, J. T. Miller, F. H. Ribeiro, R. Gounder and W. F. Schneider, *J. Am. Chem. Soc.*, 2016, **138**, 6028–6048.
75 D. Chen, Y. Yan, A. Guo, V. Rizzotto, H. Lei, Z. Qiao, H. Liang, M. Jabłońska, X. Jiang, J. Jiang, R. Palkovits, P. Chen, D. Ye and U. Simon, *Appl. Catal., B*, 2023, **322**, 122118.
76 J. Abdul Nasir, J. Guan, T. W. Keal, A. W. Desmoutier, Y. Lu, A. M. Beale, C. R. A. Catlow and A. A. Sokol, *J. Am. Chem. Soc.*, 2023, **145**, 247–259.
77 L. Chen, T. V. W. Janssens, P. N. R. Vennestrøm, J. Jansson, M. Skoglundh and H. Grönbeck, *ACS Catal.*, 2020, **10**, 5646–5656.
78 N. Zhu, Y. Shan, W. Shan, Y. Sun, K. Liu, Y. Zhang and H. He, *Environ. Sci. Technol.*, 2020, **54**, 15499–15506.
79 G. Fu, R. Yang, Y. Liang, X. Yi, R. Li, N. Yan, A. Zheng, L. Yu, X. Yang and J. Jiang, *Microporous Mesoporous Mater.*, 2021, **320**, 111060.
80 S. Ming, Z. Chen, C. Fan, L. Pang, W. Guo, K. B. Albert, P. Liu and T. Li, *Appl. Catal., A*, 2018, **559**, 47–56.
81 X. Wang, Y. Shi, S. Li and W. Li, *Appl. Catal., B*, 2018, **220**, 234–250.
82 J. Liu, S. Zhou, H. Cheng, H. Li, W. Zhu and J. Liu, *Fuel*, 2022, **318**, 123607.
83 J. Jiang, R. Zheng, Y. Jia, L. Guo, M. Huang, J. Hu and Y. Xia, *Mol. Catal.*, 2020, **493**, 111044.
84 H. Wang, T. Zhu, Y. Qiao, S. Dong and Z. Qu, *Chin. Chem. Lett.*, 2022, **33**, 5223–5227.
85 Y. Yang, J. Liu, F. Liu, Z. Wang, J. Ding and H. Huang, *Chem. Eng. J.*, 2019, **361**, 578–587.
86 L. Qi, Z. Sun, Q. Tang, J. Wang, T. Huang, C. Sun, F. Gao, C. Tang and L. Dong, *J. Hazard. Mater.*, 2020, **396**, 122459.
87 D. He, Z. Wang, D. Deng, S. Deng, H. He and L. Liu, *Mol. Catal.*, 2020, **484**, 110738.
88 J. Cheng, S. Han, Q. Ye, S. Cheng, T. Kang and H. Dai, *Microporous Mesoporous Mater.*, 2019, **278**, 423–434.
89 Z. Chen, C. Fan, L. Pang, S. Ming, P. Liu, D. Zhu, J. Wang, X. Cai, H. Chen, Y. Lai and T. Li, *Appl. Surf. Sci.*, 2018, **448**, 671–680.
90 Y. Cao, D. Fan, P. Tian, L. Cao, T. Sun, S. Xu, M. Yang and Z. Liu, *Chem. Eng. J.*, 2018, **354**, 85–92.
91 Q. Lin, S. Liu, S. Xu, P. Yao, M. Pei, H. Xu, Y. Dan and Y. Chen, *Chem. Eng. J.*, 2022, **446**, 137283.

92 R. Martínez-Franco, M. Moliner, C. Franch, A. Kustov and A. Corma, *Appl. Catal., B*, 2012, **127**, 273–280.
93 L. Ren, L. Zhu, C. Yang, Y. Chen, Q. Sun, H. Zhang, C. Li, F. Nawaz, X. Meng and F. S. Xiao, *Chem. Commun.*, 2011, **47**, 9789–9791.
94 L. Sun, M. Yang, Y. Cao, P. Tian, P. Wu, L. Cao, S. Xu, S. Zeng and Z. Liu, *Chin. J. Catal.*, 2020, **41**, 1410–1420.
95 Q. Lin, S. Liu, S. Xu, S. Xu, M. Pei, P. Yao, H. Xu, Y. Dan and Y. Chen, *Catal. Sci. Technol.*, 2021, **11**, 7640–7651.
96 Q. Wang, H. Xu, W. Huang, Z. Pan and H. Zhou, *J. Hazard. Mater.*, 2019, **364**, 499–508.
97 J. Wang, J. Liu, X. Tang, C. Xing and T. Jin, *Chem. Eng. J.*, 2021, **418**, 129433.
98 M. Chen, J. Li, W. Xue, S. Wang, J. Han, Y. Wei, D. Mei, Y. Li and J. Yu, *J. Am. Chem. Soc.*, 2022, **144**, 12816–12824.
99 M. Chen, W. Zhao, Y. Wei, J. Han, J. Li, C. Sun, D. Mei and J. Yu, *Nano Res.*, 2023, **16**, 12126.
100 Q. Wu, C. Fan, Y. Wang, X. Chen, G. Wang, Z. Qin, S. Mintova, J. Li and J. Chen, *Chem. Eng. J.*, 2022, **435**, 134890.
101 S. Han, J. Cheng, Q. Ye, S. Cheng, T. Kang and H. Dai, *Microporous Mesoporous Mater.*, 2019, **276**, 133–146.
102 J. Shi, Y. Wang, R. Duan, C. Gao, B. Wang, C. He and C. Niu, *Catal. Sci. Technol.*, 2019, **9**, 718–730.
103 Q. Lin, S. Xu, H. Zhao, S. Liu, H. Xu, Y. Dan and Y. Chen, *ACS Catal.*, 2022, **12**, 14026–14039.
104 Y. Wang, G. Li, S. Zhang., X. Zhang, X. Zhang and Z. Hao, *Chem. Eng. J.*, 2020, **393**, 124782.
105 Y. Yue, B. Liu, N. Lv, T. Wang, X. Bi, H. Zhu, P. Yuan, Z. Bai, Q. Cui and X. Bao, *ChemCatChem*, 2019, **11**, 4744–4754.
106 W. Liu, Y. Long, J. Zhang, S. Liu, Y. Zhou, X. Tong, Y. Yin, X. Li, K. Hu and J. Hu, *J. Environ. Chem. Eng.*, 2022, **10**, 108461.
107 J. Ding, X. Huang, Q. Yang, L. Wang, Y. Peng, J. Li and J. Huang, *Catal. Today*, 2022, **384–386**, 106–112.
108 Y. Ma, Y. Liu, Z. Li, C. Geng, X. Bai and D. Cao, *Environ. Sci. Pollut. Res.*, 2020, **27**, 9935–9942.
109 H. Wang, J. Jia, S. Liu, H. Chen, Y. Wei, Z. Wang, L. Zheng, Z. Wang and R. Zhang, *Environ. Sci. Technol.*, 2021, **55**, 5422–5434.
110 S. Yu, Y. Lu, F. Gao and L. Dong, *Catal. Today*, 2020, **339**, 265–273.
111 K. Cheng, W. Song, Y. Cheng, H. Zheng, L. Wang, J. Liu, Z. Zhao and Y. Wei, *RSC Adv.*, 2018, **8**, 19301–19309.
112 M.-J. Han, Y.-L. Jiao, C.-H. Zhou, Y.-L. Guo, Y. Guo, G.-Z. Lu, L. Wang and W.-C. Zhan, *Rare Met.*, 2018, **38**, 210–220.
113 B. Wang, H. Yu, M. Wang, L. Han, J. Wang, W. Bao and L. Chang, *Catal. Today*, 2021, **376**, 19–27.
114 H. Jouini, J. Martinez-Ortigosa, I. Mejri, M. Mhamdi, T. Blasco and G. Delahay, *Res. Chem. Intermed.*, 2018, **45**, 1057–1072.
115 H. Chang, X. Qin, L. Ma, T. Zhang and J. Li, *Phys. Chem. Chem. Phys.*, 2019, **21**, 22113–22120.
116 N. Zhu, Z. Lian, Y. Zhang, W. Shan and H. He, *Appl. Surf. Sci.*, 2019, **483**, 536–544.
117 Y. Shan, J. Du, Y. Yu, W. Shan, X. Shi and H. He, *Appl. Catal., B*, 2020, **266**, 118655.
118 B. Peng, K. Rappé, Y. Cui, F. Gao, J. Szanyi, M. Olszta, E. Walter, Y. Wang, J. Holladay and R. Goffe, *Appl. Catal., B*, 2020, **263**, 118359.
119 T. Zhang, F. Qiu and J. Li, *Appl. Catal., B*, 2016, **195**, 48–58.
120 Y. Wei, S. Wang, M. Chen, J. Han, G. Yang, Q. Wang, J. Di, H. Li, W. Wu and J. Yu, *Adv. Mater.*, 2023, 2302912.
121 T. Ye, Z. Chen, Y. Chen, Q. Zhong and H. Qu, *Appl. Catal. A.*, 2022, **647**, 118890.
122 T. Andana, K. Rappe, N. Nelson, F. Gao and Y. Wang, *Appl. Catal., B*, 2022, **316**, 121522.
123 H. I. Hamoud, V. Valtchev and M. Daturi, *Appl. Catal., B*, 2019, **250**, 419–428.
124 Q. Lin, S. Liu, S. Xu, P. Yao, M. Pei, H. Xu, Y. Dan and Y. Chen, *Chem. Eng. J.*, 2022, **446**, 137283.
125 X. Wu, H. Meng, Y. Du, J. Liu, B. Hou and X. Xie, *J. Catal.*, 2020, **384**, 72–87.
126 J. Zhou, P. Wang, A. Chen, W. Qu, Y. Zhao and D. Zhang, *Environ. Sci. Technol.*, 2022, **56**, 6668–6677.
127 L. Kang, L. Han, J. He, H. Li, T. Yan, G. Chen, J. Zhang, L. Shi and D. Zhang, *Environ. Sci. Technol.*, 2019, **53**, 938–945.
128 L. Jia, J. Liu, D. Huang, J. Zhao, J. Zhang, K. Li, Z. Li, W. Zhu, Z. Zhao and J. Liu, *ACS Catal.*, 2022, **12**, 11281–11293.
129 L. Yang, P. Wang, L. Yao, X. Meng, C. Q. Jia, X. Jiang and W. Jiang, *ACS Sustainable Chem. Eng.*, 2021, **9**, 987–997.
130 J.-W. Shi, Y. Wang, R. Duan, C. Gao, B. Wang, C. He and C. Niu, *Catal. Sci. Technol.*, 2019, **9**, 718–730.
131 J. He, J. Deng, J. Zhang, L. Han, Y. Shen, X. Chen, X. Hu, J. Wang and D. Zhang, *Catal. Sci. Technol.*, 2023, **13**, 2480–2492.
132 17L. Ge, A. Wang, X. Hu, J. Zhang, J. He, P. Wang, L. Han and D. Zhang, *Catal. Sci. Technol.*, 2023, **13**, 4186–4196.
133 J. He, S. Impeng, J. Zhang, J. Zhang, P. Wang and D. Zhang, *Chem. Eng. J.*, 2022, **448**, 137720.
134 F. Wang, P. Wang, J. Zhang, D. Peng, M. Wei and D. Zhang, *Chin. Chem. Lett.*, 2023, 108800.
135 X. Wang, Y. Liu and Z. Wu, *Chem. Eng. J.*, 2020, **382**, 122941.
136 J. Chen, R. Zhao and R. Zhou, *ChemCatChem*, 2018, **10**, 5182–5189.
137 Y. Jangjou, Q. Do, Y. Gu, L.-G. Lim, H. Sun, D. Wang, A. Kumar, J. Li, L. C. Grabow and W. S. Epling, *ACS Catal.*, 2018, **8**, 1325–1337.
138 R. Yu, Z. Zhao, S. Huang and W. Zhang, *Appl. Catal., B*, 2020, **269**, 118825.
139 R. Yu, H. Kong, Z. Zhao, C. Shi, X. Meng, F. S. Xiao, T. De Baerdemaeker, A. N. Parvulescu, U. Müller and W. Zhang, *ChemCatChem*, 2022, **14**, e202200228.
140 Q. Yan, Y. Nie, R. Yang, Y. Cui, D. O'Hare and Q. Wang, *Appl. Catal., A*, 2017, **538**, 37–50.
141 Q. Yan, S. Chen, C. Zhang, Q. Wang and B. Louis, *Appl. Catal., B*, 2018, **238**, 236–247.
142 X. Liu, X. Wu, D. Weng and Z. Si, *Catal. Commun.*, 2015, **59**, 35–39.

143 C. Wang, W. Yan, Z. Wang, Z. Chen, J. Wang, J. Wang, J. Wang, M. Shen and X. Kang, *Catal. Today*, 2020, **355**, 482–492.
144 F. Gao, Y. Wang, N. M. Washton, M. Kollár, J. Szanyi and C. H. F. Peden, *ACS Catal.*, 2015, **5**, 6780–6791.
145 C. Fan, Z. Chen, L. Pang, S. Ming, C. Dong, K. Brou Albert, P. Liu, J. Wang, D. Zhu, H. Chen and T. Li, *Chem. Eng. J.*, 2018, **334**, 344–354.
146 N. Zhu, W. Shan, Y. Shan, J. Du, Z. Lian, Y. Zhang and H. He, *Chem. Eng. J.*, 2020, **388**, 124250.
147 P. Wang, L. Yan, Y. Gu, S. Kuboon, H. Li, T. Yan, L. Shi and D. Zhang, *Environ. Sci. Technol.*, 2020, **54**, 6396–6405.
148 X. Wang, Q. Cong, L. Chen, Y. Shi, Y. Shi, S. Li and W. Li, *Appl. Catal., B*, 2019, **246**, 166–179.
149 H. Li, J. Miao, Q. Su, Y. Yu, Y. Chen, J. Chen and J. Wang, *J. Mater. Sci.*, 2019, **54**, 14707–14719.
150 Z. Chen, M. Shen, C. Wang, J. Wang, J. Wang and G. Shen, *Catalysts*, 2021, **11**, 979.
151 S. Y. Choi, R. Purbia, H. J. Kim, J.-K. Kim, S.-W. Kim, J. Mo, B. Ye, B. Jeong, D. H. Lee, D. Kim, H. Park, H.-D. Kim and J. M. Baik, *Appl. Surf. Sci.*, 2023, **623**, 157088.
152 S. Raja, M. S. Alphin, L. Sivachandiran, P. Singh, D. Damma and P. G. Smirniotis, *Fuel*, 2022, **307**, 121886.
153 X. Yong, C. Zhang, M. Wei, P. Xie and Y. Li, *J. Catal.*, 2021, **394**, 228–235.
154 W. Kang, B. Choi and H. Kim, *J. Ind. Eng. Chem.*, 2013, **19**, 1406–1412.
155 T. Usui, Z. Liu, H. Igarashi, Y. Sasaki, Y. Shiramata, H. Yamada, K. Ohara, T. Kusamoto and T. Wakihara, *ACS Omega*, 2019, **4**, 3653–3659.
156 H. Tian, Y. Ping, Y. Zhang, Z. Zhang, L. Sun, P. Liu, J. Zhu and X. Yang, *J. Hazard. Mater.*, 2021, **416**, 126194.
157 L. Sun, M. Yang, L. Cao, Y. Cao, S. Xu, D. Zhu, P. Tian and Z. Liu, *Microporous Mesoporous Mater.*, 2020, **309**, 110585.
158 Y. Ma, H. Zhao, C. Zhang, Y. Zhao, H. Chen and Y. Li, *Catal. Today*, 2020, **355**, 627–634.